JOURNAL OF PETROLOGY | VOLUME 54 | NUMBER 1 | PAGES 149–182 | 2013 | doi:10.1093/petrology/egs066

Crustal Differentiation Processes at Krakatau Volcano, Indonesia

MÀIRI F. GARDNER[1], VALENTIN R. TROLL[2]*, JOHN A. GAMBLE[1,3], RALF GERTISSER[4], GARRET L. HART[5], ROB M. ELLAM[6], CHRIS HARRIS[7] AND JOHN A. WOLFF[5]

[1]DEPARTMENT OF GEOLOGY, UNIVERSITY COLLEGE CORK, CORK, IRELAND

[2]DEPARTMENT OF EARTH SCIENCES, CEMPEG, UPPSALA UNIVERSITY, 75236 UPPSALA, SWEDEN

[3]SCHOOL OF GEOGRAPHY, ENVIRONMENT AND EARTH SCIENCE, VICTORIA UNIVERSITY OF WELLINGTON, WELLINGTON 6140, NEW ZEALAND

[4]SCHOOL OF PHYSICAL AND GEOGRAPHICAL SCIENCES, KEELE UNIVERSITY, KEELE, STAFFORDSHIRE ST5 5BG, UK

[5]DEPARTMENT OF GEOLOGY, WASHINGTON STATE UNIVERSITY, PULLMAN, WA, 99164-2812, USA

[6]SCOTTISH UNIVERSITIES ENVIRONMENT RESEARCH CENTRE, EAST KILBRIDE, G75 0QF, UK

[7]DEPARTMENT OF GEOLOGICAL SCIENCES, UNIVERSITY OF CAPE TOWN, RONDEBOSCH, 7701, SOUTH AFRICA

RECEIVED OCTOBER 25, 2009; ACCEPTED AUGUST 30, 2012
ADVANCE ACCESS PUBLICATION OCTOBER 31, 2012

Anak Krakatau is a basaltic andesite cone that has grown following the famous caldera-forming 1883 eruption of Krakatau. It breached sea level in 1927 and since the 1950s has been growing at an average rate of ~8 cm a week. We present new major and trace element data combined with whole-rock $\delta^{18}O$, Sr and Nd isotope data for 1883, 1993 and 2002 Krakatau eruptive products and the surrounding crust. Bombs erupted from Anak Krakatau during 2002 contain frothy metasedimentary and plutonic xenoliths that show variable degrees of thermal metamorphism, plastic deformation and partial melting. Contact-metamorphic minerals such as cordierite and tridymite in metasedimentary xenoliths are consistent with high-temperature metamorphism and incorporation at mid- to upper-crustal depth. Energy-constrained assimilation and fractional crystallization modelling of whole-rock data suggests that the Anak Krakatau magmas have a genetic relationship with the 1883 eruption products. The geochemical impact of crustal contaminants on whole-rock compositions is apparently small, and we conclude that low levels of assimilation of a quartzo-feldspathic sediment are recorded in Anak Krakatau magmas. Plagioclase phenocrysts from the 2002 eruption exhibit disequilibrium textures and complex compositional zoning, however, and are also isotopically variable with a total range in $^{87}Sr/^{86}Sr$ of 0·7043–0·7048 as determined by in situ laser ablation inductively coupled plasma mass spectrometry. This suggests that although shallow crustal assimilation appears to have had a limited effect on whole-rock chemistry, a complex late-stage differentiation history is recorded within the magma's cargo of crystals and xenoliths.

KEY WORDS: *Anak Krakatau; plagioclase; crustal xenoliths; assimilation and fractional crystallization; isotope micro-analysis*

INTRODUCTION

Anak Krakatau, located in the Sunda Strait between Java and Sumatra, is a post-collapse cone that has grown inside the caldera formed by the 1883 eruption of Krakatau volcano. The volcano has an infamous past and with the present continuation of activity (e.g. in 2006 and 2008) it also poses a potential hazard in the future through its location in a busy shipping lane between Java and Sumatra and its proximity to Jakarta, a major population centre. Previous work on the volcanic complex has focused on whole-rock data from the 1883 eruption (Mandeville *et al.*, 1996) and single samples from eruptions of Anak Krakatau through the 1970s and 1980s (Nishimura *et al.*, 1980; Oba *et al.*, 1982; Camus *et al.*, 1987), as well as forming part of wider, along-arc studies (Turner & Foden, 2001; Woodhead

*Corresponding author: valentin.troll@geo.uu.se

et al., 2001). However, a growing abundance of *in situ* isotope studies have revealed that bulk-rock analyses may disguise the complexity of evolutionary processes in intermediate volcanic rocks, particularly those of arc-type volcanoes (e.g. Davidson & Tepley, 1997; Tepley *et al.*, 1999, 2000; Browne *et al.*, 2006; Chadwick *et al.*, 2007; Morgan *et al.*, 2007). In this respect, a whole-rock composition merely represents an integrated average of the source and subsequent magmatic open-system modifications, typically involving not only fractional crystallization, but also degassing, convection and crustal contamination, as well as magma mixing and mingling. To improve our understanding of the processes within active volcanic systems, and to further our knowledge on what transforms a mantle-derived magma *en route* to the surface, it is imperative that we identify the nature and extent of these pre-eruptive crustal processes.

As a stable crystallizing phase over a wide range in temperatures and pressures, plagioclase is a common mineral in many mafic to intermediate magmatic systems and retains a record of changing magmatic conditions during growth (e.g. Pearce & Kolisnik, 1990; Stamatelopoulou-Seymour *et al.*, 1990; Blundy & Shimizu, 1991; Singer *et al.*, 1995; Tepley *et al.*, 2000; Ginibre *et al.*, 2002; Ruprecht & Wörner, 2007). The major compositional variations of plagioclase are controlled by NaSi–CaAl coupled substitution, and are determined by P–T–X variations (Grove *et al.*, 1984). Trace element concentrations, in turn, follow constraints of crystal–liquid partition coefficients and their distribution in crystals is further influenced by varying rates of diffusion in the solid state (Zellmer *et al.*, 1999, 2003; Costa *et al.*, 2003). Diffusion rates for NaSi–CaAl are sufficiently slow relative to the timescales of magmatic events (Grove *et al.*, 1984; Baschek & Johannes, 1995; Wallace & Bergantiz, 2005; Pichavant *et al.*, 2007) that anorthite zonation and resorption–dissolution surfaces can be interpreted as dominantly representing changes in magmatic conditions experienced by the phenocrysts during growth (Pearce & Kolisnik, 1990; Davidson & Tepley, 1997; Troll *et al.*, 2004; Browne *et al.*, 2006; Humphreys *et al.*, 2006; Chadwick *et al.*, 2007; Ruprecht & Wörner, 2007).

In an evaluation of the petrogenetic links between the andesites and rhyolites of New Zealand, Price *et al.* (2005) argued that the genesis of andesites reflected the interaction of mantle melts with crustal partial melts and restite materials, a concept also developed by Annen *et al.* (2006). Repeated injection of mantle-derived magmas into a 'deep-crustal hot zone' progressively prepares a situation suitable for the production of large, intermediate to silicic magma bodies by melting and homogenization. These magmas may rise to shallow levels where they aggregate and potentially erupt in large, caldera-forming events such as at Toba, Taupo or, in fact, the Krakatau 1883 event. However, stochastic modelling of dyke intrusions (Dufek & Bergantz, 2005) raises some doubt over the capability of basalt fluxes to melt significant volumes of the crust. In contrast, Beard *et al.* (2005) have suggested that incorporation of solid matter (e.g. xenocrysts) will reduce the energy constraints for crustal assimilation, allowing efficient magma differentiation owing to high crustal uptake. Alternatively, Bachman & Bergantz (2004, 2008) have proposed that compaction of crystal mush zones may force the ascent of silicic interstitial melts (>65 wt % SiO_2). Although most models envisage mid- to lower-crustal focus zones (e.g. MASH model or lower crustal hot zones; Hildreth & Moorbath, 1988; Dufek & Bergantz, 2005; Annen *et al.*, 2006), there is still considerable uncertainty concerning the depths at which magmas develop their compositional, intra-crystal textural and isotopic heterogeneity (Brophy, 1991; Reubi & Blundy, 2009). Whereas fractional crystallization has been invoked as the dominant process controlling the evolution of Anak Krakatau magmas (Camus *et al.*, 1987), a closed-system evolution has been called into question with the identification of frothy metasedimentary xenoliths (Mandeville *et al.*, 1996; this study), measurements of helium isotope variations in clinopyroxene (Gasparon *et al.*, 1994) and fumarole gas emissions (Blythe *et al.*, 2009).

To distinguish between various differentiation processes (e.g. crustal contamination and fractional crystallization), we investigated intra-crystal Sr isotope ratios of Anak Krakatau plagioclase using laser ablation inductively coupled plasma mass spectrometry (LA-ICP-MS; Davidson *et al.*, 2001; Ramos *et al.*, 2004). Fundamental to the method of crystal isotope stratigraphy (CIS; Davidson & Tepley, 1997; Davidson *et al.*, 2007) is the premise that isotopic ratios are a measure of the state of equilibrium between crystal and liquid at an instant in time and are immune to change by purely physical processes such as simple fractional crystallization. A change in isotopic signature can thus be achieved only by addition of an isotopically distinct component, through a process such as crustal assimilation or magma mixing (e.g. Knesel *et al.*, 1999; Tepley *et al.*, 1999; Davidson *et al.*, 2001; Ramos *et al.*, 2004, 2005; Francalanci *et al.*, 2005; Chadwick *et al.*, 2007; Charlier *et al.*, 2007; Deegan *et al.*, 2010).

Here, we present new whole-rock major and trace element and Sr, Nd and O isotopic data for rocks from the Krakatau volcanic complex. In particular, we focus on bombs from intermittent strombolian activity during the 2001–2002 eruptive episode of Anak Krakatau to investigate compositional diversity within a narrow time interval. We then assess these data in conjunction with *in situ* laser ablation $^{87}Sr/^{86}Sr$ measurements of plagioclase phenocrysts and whole-rock data from the 1883 and 1993 eruptions to evaluate the extent of magma–crust interaction at Krakatau through time.

GEOLOGICAL SETTING AND ERUPTIVE HISTORY

The Sunda Arc is an active volcanic belt that extends over 5600 km from the Andaman Islands in the NW to the Banda Arc in the east, making it one of the largest subduction systems on Earth. Magmatism results from the northward subduction of the Indo-Australian plate beneath the Eurasian plate (Fig. 1, inset a), where convergence between both oceanic and continental lithosphere leads to considerable variations in fore-arc geometry and magmatism along and across strike (Jarrard, 1986; Newcomb & McCann, 1987; Kopp *et al.*, 2001; Turner & Foden, 2001; Woodhead *et al.*, 2001).

The Krakatau volcanic complex is located in the Sunda Strait, *c.* 40 km west of Java, and is part of a NNE–SSW-trending lineament of Quaternary volcanic edifices that lies approximately perpendicular to the Java trench (Fig. 1). The Sunda Strait is an area of extensive faulting and rifting associated with the transition from oblique subduction beneath Sumatra to near orthogonal subduction under Java (Huchon & Le Pichon, 1984; Diament *et al.*, 1990; Harjono *et al.*, 1991; Malod *et al.*, 1995; Malod & Kemal, 1996; Schlüter *et al.*, 2002). This geodynamic complexity has produced one of the most tectonically and volcanically active areas in Indonesia (Huchon & Le Pichon, 1984). For example, the 1883 event at 'Krakatoa' (as it was originally misspelt in news telegrams) was one of the largest explosive eruptions in historical times (Self & Rampino, 1981; Simkin & Fiske, 1983; Sigurdsson *et al.*, 1991; Mandeville *et al.*, 1996).

The transtensional tectonic regime of the Sunda Strait is primarily due to the northwestward displacement of a Sumatra fore-arc sliver plate along the dextral fault system of Central Sumatra (Huchon & Le Pichon, 1984). Block faulting of the basement, crustal thinning and active normal faults have created space locally for up to 6 km of graben fill (Lelgemann *et al.*, 2000) and total extension over the Strait is now estimated at 50–100 km (Huchon & Le Pichon, 1984; Lassal *et al.*, 1989; Diament *et al.*, 1992; Malod & Kemal, 1996; Susilohadi *et al.*, 2009). Schlüter *et al.* (2002) reported bathymetric and seismic data acquired from the area immediately south of the present Krakatau volcanic complex, identifying a pull-apart basin of Middle Miocene age (the Krakatau Basin) overlain by Upper Miocene, Pliocene and Pleistocene sediments (described below). The currently active Krakatau complex is situated within this basin at the intersection of an active fault (oriented N150°E; Deplus *et al.*, 1995) with the volcanic line running from Panaitan Island to Rajabasa (oriented N20°E), and with seismic activity extending from very shallow depths of 3–8 km to *c.* 100 km below Anak Krakatau (Harjono *et al.*, 1989, 1991; Hanuš *et al.*, 1996; Špičák *et al.*, 2002; Hoffmann-Rothe *et al.*, 2006; Ibs-von Seht, 2008; Jaxybulatov *et al.*, 2011). Micro-seismicity studies (Harjono *et al.*, 1989, 1991) suggest that the crust extends to a depth of *c.* 22 km.

In previous work (e.g. Mandeville *et al.*, 1996; Dahren *et al.*, 2012), the crustal stratigraphy beneath the Krakatau complex has been inferred from the 3005 m deep Pertamina-Aminoil well, just 30 km SE of the volcano (C-1SX in Fig. 1). Considering the widespread faulting in the area, this well may not represent the depth of single stratigraphic units below Anak Krakatau accurately, but it can be taken as an indication of the rock-types present in the regional sedimentary basin with a crude approximation of their local thickness. Well C-1SX penetrated an apparently continuous Quaternary marine succession (555 m thick), overlying 2450 m of Upper Pliocene sedimentary rocks composed of mostly clays and claystones interbedded with quartz sandstone, siltstone, tuffs and altered volcaniclastic rocks (Noujaim, 1976; De Neve & Sukardjono, 1985). The 555 m Quaternary marine sedimentary sequence contains an abundance of marine fossils of benthic fauna and foraminifera (i.e. calcium carbonate) within siliciclastic and argillaceous sediments (Nishimura *et al.*, 1986), and indicates a general shallowing from a deeper, outer sublittoral environment of deposition (from 555 to 244 m) to an inner sublittoral one (244 to 0 m).

Thick, siliciclastic successions within the Krakatau Basin are also recorded in wells B-1SX and D-1SX (Fig. 1), which terminate in Late Pliocene sediments at a depth of 1526 m and 2448 m, respectively (Lunt *et al.*, 2009).

The three drill holes in the Krakatau Basin failed to reach Miocene strata, although potential onshore equivalents can be found at outcrops around Ujung Kulon, Panaitan Island and near Telukbetung (Fig. 1). Early Miocene volcanic breccias, andesitic lavas, pillow lavas, calcareous tuffs and limestones, partly interbedded with marine turbiditic sediments on both southern Sumatra and Java (e.g. Susilohadi *et al.*, 2009), suggest that similar geological settings existed across the Strait prior to initiation of the extensional regime.

Other exploratory oil wells to the NW of Java and SE of Sumatra were drilled through to a proposed basement of (K–Ar dated) Cretaceous continental crust including granites and quartz monzonites (Hamilton, 1979). Granitic xenoliths have been identified in the 1883 pyroclastic flow units on Sertung (Oba *et al.*, 1982) and dioritic fragments have been found within the modern lavas (this study). Although similarities have been drawn between the plutonic inclusions in the Krakatau volcanic products and West Malayan granites (Oba *et al.*, 1992), analogous onshore basement rocks are difficult to identify as the boundary between the East Malaya and the SW Borneo terranes of Sundaland lies in close proximity to the Sunda Strait (Metcalfe, 1990; Wakita, 2000).

Prior to August 1883, Krakatau Island was 9 km long and 5 km wide (marked by dashed outline in Fig. 1, inset

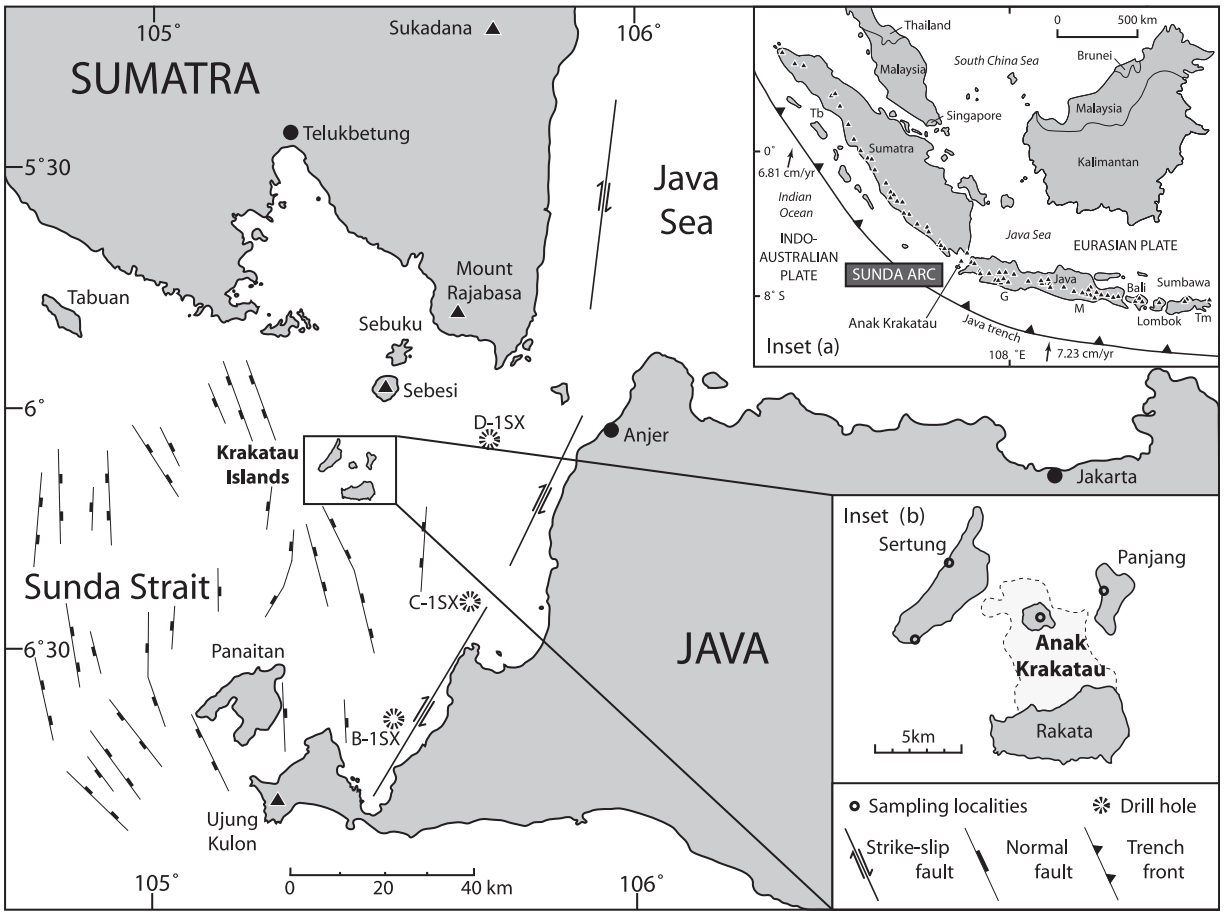

Fig. 1. Geological setting and location map of the Sunda Strait and of the wider Sunda Arc area (inset a) with the current configuration of the Krakatau volcanic complex (inset b). Map and oil well location based on Mandeville *et al.* (1996) and Lunt *et al.* (2009), with faults from Schlüter *et al.* (2002) and Susilohadi *et al.* (2009). Tb, Toba; G, Galunggung; M, Merapi; Tm, Tambora.

b), consisting of three volcanic vents: 813 m Rakata, 445 m Danan and ~120 m Perbuwatan (Verbeek, 1884, 1885; Self & Rampino, 1981; see Table 1). The events of 1883 produced ~12·5 km^3 dense rock equivalent (DRE) of magma in a series of eruptions commencing on 20 May and culminating in the cataclysmic caldera-forming eruption of 26–27 August (Verbeek, 1884, 1885; Van Bemmelen, 1949; Mandeville *et al.*, 1996). The only exposed remnant of this pre-1883 edifice of Krakatau is the dissected cone of Rakata, previously the southernmost peak of the volcanic complex (see Table 1). The three peaks were aligned roughly SE–NW and situated along a fissure within a prehistoric, ~7 km wide caldera, at present marked by the islands of Sertung and Panjang (Escher, 1919; Stehn, 1929).

The contemporary Krakatau volcanic complex consists of four islands: Rakata, Sertung, Panjang and Anak Krakatau. Anak Krakatau, the 'child' of Krakatau, breached sea level in 1928 and has now reached a height of ~315 m (Hoffman-Rothe *et al.*, 2006). The post-collapse cone has grown from the geographical centre of the 1883 caldera, which, prior to the renewal of activity, lay at an average depth of 263 m below sea level (Verbeek, 1885; Stehn, 1929; van Bemmelen, 1949). The growth rate of Anak Krakatau is one of the fastest on Earth and since the 1950s it has increased in height by an average of 4–4·25 m a^{-1} (~8 cm per week; Sudradjat, 1982). Present-day activity is characterized by strombolian to vulcanian eruptions of basaltic andesite magma with associated localized lava flows and cone-like tephra deposits. A brief historical record of eruption styles and compositions can be seen in Table 1.

Harjono *et al.* (1989) noted that structural effects beneath the Krakatau edifice are dominated by compression at <4 km depth and extension at >4 km and, using a combination of 14 local earthquakes in 1984, constructed a seismic attenuation model that identified two low-velocity zones beneath Anak Krakatau. The lower zone from ~22 km to at least 32 km is interpreted to be a very wide magma body associated with the extensional nature of the Strait, whereas the upper zone at ≤7 km is thought to consist of

Table 1: Eruption history for Krakatau volcanic complex

Age	Activity	Products	References
Proto-Krakatau	Growth of large volcano	Hypersthene andesite	1, 2, 3, 4
	Caldera-forming eruption leaving Rakata, Sertung, Panjang and Poolsche Hoed	Dacitic pumice	1, 2, 3, 4, 5
Pre-1883	Growth of Rakata cone to ~800 m, dykes cut through the cone	Basalt and andesite	3, 4
	Vulcanian and strombolian activity, growth of Danan and Perbuwatan	Andesite and dacite pumices	3, 4, 5, 6
	Pyroclastic fall, surge and flow deposits	Dacitic pumice	5
	Strombolian eruption	Basalt	5
1883	Caldera-forming eruption from zoned rhyodacite magma chamber	Banded rhyodacite pumice and obsidian	1, 2, 7, 8, 9
1927–1979	Intermittent vulcanian and strombolian eruptions, with some lava flows	Basaltic andesite	10
1981	Vulcanian activity	Silicic andesite	10, 11
1988 to present day	Intermittent central and flank vent strombolian eruptions and lava flows	Basaltic andesite	

References: (1) Verbeek (1984); (2) Verbeek (1885); (3) Escher (1928); (4) Stehn (1929); (5) Beauregard (2001); (6) Judd (1889); (7) Van Bemmelen (1949); (8) Self & Rampino (1981); (9) Mandeville *et al*. (1996); (10) Oba *et al*. (1982); (11) Camus *et al*. (1987).

a number of irregular pockets of magma. This array of shallow pockets might nevertheless make up a sufficiently large integrated volume to replicate the 1883 eruption, and is likely to be connected to the deeper chamber complex (e.g. Dahren *et al*., 2012).

SAMPLE SELECTION AND ANALYTICAL METHODS

Sample selection and preparation

Samples of basaltic andesite lava as well as metasedimentary and plutonic xenoliths from the 2002 eruptive episode were collected in March 2005 from the vicinity of the old crater rim (Table 2), close to the new summit of Anak Krakatau (just prior to the increase in activity in April and May 2005). Hand specimen-sized samples were collected from bombs that range in size up to ~3 m^3. Xenoliths (up to 20 cm across) are frequently found within the lava samples. One sample was also collected from the 1993 lava flow on the northern shore of the island (see Table 2 for sample descriptions).

The studied 1883 pumices and olive-coloured obsidians were sampled from cliff sections through the pyroclastic flow deposits on the neighbouring islands of Panjang and Sertung (see localities in Fig. 1b inset and Table 2). Mandeville *et al*. (1996) reported that of the 1883 eruptive products, highly vesiculated white pumices make up over 85%, light to dark grey pumices make up ~4% and strongly banded pumices <1%. Olive-coloured obsidian constitutes ~1–5% and lithic fragments another 1–5% of the total deposits blanketing Panjang and Sertung islands.

In addition to these juvenile eruptive components, we sampled lithic fragments from within the 1883 deposits in the western cliffs of Sertung. These consist of hydrothermally altered pre-1883 basaltic andesites (e.g. samples K.S.IC-03, K.S.IC-06 and K.S.IC-07), carbonate mudstones (e.g. K.S.SC-05 and K.S.SC-06) and immature siltstones and sandstones containing baked foraminifera and shell fragments (K.S.SC-01 and K.S.SC-03).

Samples were prepared for whole-rock major and trace element analysis by removing weathered surfaces prior to chipping and jaw-crushing. Samples were then washed in distilled water, dried and milled to powder in a tungsten-carbide disc-mill at Trinity College Dublin.

Analytical methods

The whole-rock mineralogy of eight fine-grained xenoliths and crustal lithic samples was determined by X-ray diffraction (XRD) at the Geochemistry Laboratory in the Geology Department of Trinity College, Dublin, using a Phillips PW 1720 X-ray generator and a Phillips PW 1050/25 diffractometer. The minerals present in each sample were determined by standard XRD methods using Ni-filtered Cu Kα radiation following the techniques described by Donoghue *et al*. (2008).

Table 2: Sample descriptions

Group	Sample	Description	Sampling locality
Anak	AK.LF	basaltic andesite from 1993 lava flow	Anak: shoreline
Anak	AK.Xla-05	basaltic andesite lava bomb with xenolith	Anak: old crater rim
Anak	AK.Xlc-01	basaltic andesite lava bomb with xenolith	Anak: old crater rim
Anak	AK.Xlc-03	basaltic andesite lava bomb with xenolith	Anak: old crater rim
Anak	AK.Xlc-11	basaltic andesite lava bomb with xenolith	Anak: old crater rim
Anak	AK.Xlc-13	basaltic andesite lava bomb with xenocryst	Anak: old crater rim
Anak	AK.Xlc-1	basaltic andesite lava bomb with xenolith	Anak: old crater rim
Anak	AK.Xlc-25	basaltic andesite lava bomb with xenolith	Anak: old crater rim
Anak	AK.Xlf-20	basaltic andesite lava bomb with xenolith	Anak: old crater rim
Anak	AK-1	basaltic andesite lava bomb	Anak: old crater rim
Anak	AK.CS-2	basaltic andesite lava bomb	Anak: old crater rim
Anak	AK.L-01	basaltic andesite lava bomb	Anak: old crater rim
Xenolith	AK.Xla-03	green-coloured, altered igneous xenolith	Anak: old crater rim
Xenolith	AK.Xla-05 x	green-coloured, altered mafic xenolith	Anak: old crater rim
Xenolith	AK.Xlf-02	frothy metasedimentary xenolith	Anak: old crater rim
Xenolith	AK.Xlf-05	glassy, partially melted crystalline xenolith	Anak: old crater rim
Xenolith	AK.Xlf-06	frothy, partially melted crystalline xenolith	Anak: old crater rim
Xenolith	AK.Xlf-11	frothy metasedimentary xenolith	Anak: old crater rim
Xenolith	AK.Xlf-15	frothy metasedimentary xenolith	Anak: old crater rim
Xenolith	AK.Xlf-17	frothy metasedimentary xenolith	Anak: old crater rim
Xenolith	AK.Xlf-20	frothy metasedimentary xenolith	Anak: old crater rim
Xenolith	AK.Xlf-23	frothy metasedimentary xenolith	Anak: old crater rim
Xenolith	AK.Xlf-27	blue-coloured metasedimentary xenolith	Anak: old crater rim
Xenolith	AK.Xlf-28	frothy metasedimentary xenolith	Anak: old crater rim
Xenolith	AK.Xlf-31	yellow-coloured foamy xenolith	Anak: old crater rim
Xenolith	AK.Xlf-32	frothy metasedimentary xenolith	Anak: old crater rim
Xenolith	AK.Xlf-42	frothy metasedimentary xenolith	Anak: old crater rim
1883	K.P.Ob-01	pre-1883 basaltic feldspar porphyry	Panjang: west coast cliff
1883	K.P.WP-01	1883 white pumice	Panjang: west coast cliff
1883	K.P.WP-02	1883 white pumice	Panjang: west coast cliff
1883	K.S.Ob-01	1883 olive obsidian	Sertung: SE cliff
1883	K.S.Ob-02	1883 olive obsidian	Sertung: SE cliff
1883	K.S.Ob-15	1883 olive obsidian	Sertung: SE cliff
1883	K.S.P-03	1883 white to grey banded pumice	Sertung: west coast cliff
1883	K.S.P-09	1883 white–olive pumice	Sertung: SE cliff
1883	K.S.P-15	1883 grey pumice	Sertung: west coast cliff
Crustal lithic	K.S.IC-03	igneous clast in 1883 deposits	Sertung: west coast cliff
Crustal lithic	K.S.IC-06	igneous clast in 1883 deposits	Sertung: west coast cliff
Crustal lithic	K.S.IC-07	layered silty lithic clast in 1883 deposits	Sertung: west coast cliff
Crustal lithic	K.S.SC-01	limestone lithic clast in 1883 deposits	Sertung: west coast cliff
Crustal lithic	K.S.SC-02	limestone lithic clast in 1883 deposits	Sertung: west coast cliff
Crustal lithic	K.S.SC-03	silty lithic clast in 1883 deposits	Sertung: west coast cliff
Crustal lithic	K.S.SC-05	chalky lithic clast in 1883 deposits	Sertung: west coast cliff
Crustal lithic	K.S.SC-06	chalky lithic clast in 1883 deposits	Sertung: west coast cliff
Crustal lithic	K.S.SC-07	layered silty lithic clast in 1883 deposits	Sertung: west coast cliff

At ~200 m (a.s.l.) the old crater rim of Anak Krakatau lies to the west of the present crater and represents the summit of Anak during the 1960s.

Major and trace element concentrations of 29 samples were determined by X-ray fluorescence (XRF) on fused beads using an automated Philips PW 1480 spectrometer at IFM-GEOMAR Research Centre, Kiel, Germany. Samples were dried at 110°C before analysis, and then heated to ~1100°C to determine loss on ignition (LOI). All analyses were performed using a Rh-anode X-ray tube and calibration was performed using international geological reference materials (JA-2, JB-2, JB-3 and JR-1) as monitors. Reference material analyses have been reported by Abratis *et al.* (2002).

A complementary set of seven XRF analyses was made at Edinburgh University following the techniques described by Fitton *et al.* (1998) and with modifications noted by Fitton & Godard (2004). Analytical precision and accuracy are comparable with the values reported by Fitton *et al.* (1998).

Rare earth elements (REE) and Hf, Ta, Pb, Th, and U were determined by inductively coupled plasma mass spectrometry (ICP-MS, VG PlasmaQuad II) at the Scottish Universities Environmental Research Centre (SUERC), East Kilbride. Analyses of international reference materials BCR-1 and BCR-2 were made throughout sample batches according to the methods of Olive *et al.* (2001) and are within error of reported values therein.

Isotopic analyses for Sr and Nd by thermal ionization mass spectrometry (TIMS) were also obtained at SUERC in multi-dynamic mode on a VG Sector 54-30 mass spectrometer. Samples and reference materials were processed through conventional HF–HNO_3–HCl dissolution before Sr and middle REE (MREE) were separated by standard cation exchange column chemistry and Nd was further purified on an anion column. Sr and Nd were then loaded onto Ta and Re filaments, respectively. Total procedure blanks were less than 100 pg, and therefore negligible for both Sr and Nd. Mass fractionation was corrected using an exponential law assuming $^{86}Sr/^{88}Sr = 0{\cdot}1194$ and $^{146}Nd/^{144}Nd = 0{\cdot}7219$. For $^{87}Sr/^{86}Sr$, NIST SRM $987 = 0{\cdot}710254 \pm 18$ to 2SD [within error of $0{\cdot}710248 \pm 23$ to 2SD ($n = 427$) reported by Thirlwall (1991)] and for $^{143}Nd/^{144}Nd$, $J + M = 0{\cdot}511504 \pm 9$ to 2SD. This is indistinguishable from the laboratory long-term mean of $0{\cdot}511500 \pm 10$. In addition to the $^{87}Sr/^{86}Sr$ and $^{143}Nd/^{144}Nd$ ratios obtained at SUERC, we also analysed 12 samples for $^{87}Sr/^{86}Sr$ on the ThermoFinnigan Neptune multicollector (MC)-ICP-MS system in the GeoAnalytical Lab at Washington State University, with multiple analyses of reference material NIST SRM 987 averaging $0{\cdot}710265 \pm 15$ to 2SD ($n = 6$).

A conventional vacuum extraction line employing ClF_3 at the University of Cape Town was used to measure whole-rock $\delta^{18}O$ values (Borthwick & Harmon, 1982; Harris *et al.*, 2000). Two samples of NBS 28 were analysed with every eight samples and repeated analysis of the reference materials gave an analytical error of $< \pm 0{\cdot}15‰$. Data are reported in the familiar delta notation (δ) relative to SMOW and raw data were normalized to the SMOW scale using a value of +9·64‰ for NBS 28.

Electron microprobe (EMP) analyses on carbon-coated polished thick-sections (~150 μm) were performed at the Open University, Milton Keynes on a CAMECA SX 100 microprobe with internal 'PAP' correction (Pouchou & Pichoir, 1991). Major and minor element analysis (Si, Ti, Al, Fe, Mg, Ca, Na, K, Ba and Sr) of plagioclase crystals was performed using an accelerating potential of 20 kV, a beam current of 20 nA, and a 10 μm diameter defocused electron beam. Peak counting times of 20 s were chosen for all elements except Ba and Sr, for which extended counting times of 40 s were used. Sodium was analysed first, and with the same 10 μm diameter defocused beam, to avoid time-dependent loss in intensity of the Na Kα peak. Natural silicate mineral and synthetic standards, mostly supplied by CAMECA, were used as primary standards to calibrate the instrument and as secondary, in-run standards to monitor precision and accuracy during analyses. All crystals studied were zoned and plagioclase phenocrysts displaying suitably wide zones for laser ablation were selected for further isotopic analysis.

Laser ablation analyses were performed at Washington State University to obtain $^{87}Sr/^{86}Sr$ isotope ratios of single zones in plagioclase crystals using a Finnigan Neptune multi-collector ICP-MS system combined with a New Wave UP-213 Nd:YAG laser ablation system (pulse rate 20 Hz, 80 μm spot size, 3 μm depth per pass, 0·625 mJ, 11·9 J/cm^2) following the techniques, settings and data reduction procedures reported by Ramos *et al.* (2004). During the analytical period, precision was monitored by multiple analyses of an in-house reference material ($^{87}Sr/^{86}Sr = 0{\cdot}70405 \pm 7$, $n = 8$).

To confirm the suitability of the plagioclase crystals for LA-ICP-MS $^{87}Sr/^{86}Sr$ analysis, Rb/Sr ratios were calculated from data obtained by *in situ* analyses of trace elements determined at Washington State University using a high-resolution single-collector ICP-MS system (Finnigan Element2) combined with a New Wave UP-213 laser ablation system (20 Hz, 30 μm spot size, no repeat passes, 0·078 mJ, helium rate ~60·3, reference materials of BCR2 and BIR). Calculated Rb/Sr ratios within the studied plagioclase phenocrysts are typically <0·002, considerably below the threshold of 0·01, above which Rb interferences cause significant deterioration in the quality of $^{87}Sr/^{86}Sr$ determinations by LA-ICP-MS (Davidson *et al.*, 2001).

RESULTS

Mineralogy and petrography

The 2002 Anak Krakatau bomb and lava samples are porphyritic basaltic andesites with phenocrysts of plagioclase, clinopyroxene, orthopyroxene, apatite, and Fe–Ti oxides

in minor proportions plus a significant amount of xenolithic material (Fig. 2). Modal analyses of polished thin sections of lava samples are given in Table 3.

Plagioclase feldspar phenocrysts in the 2002 basaltic andesites show significant variations in composition and texture. A thin section of sample AK1 was selected for EMP analysis as the plagioclase phenocrysts from the single section displayed a range of compositions from An_{44} to An_{90} that is reflective of the entire observed spectrum (Fig. 3a and b). Petrographic analysis and EMP profiles across plagioclase crystals show overall normal zonation, with rare oscillatory or reverse zoning. The phenocrysts also commonly display complex zonation with sieve-textured zones of partial resorption, truncation of growth zones and rounded edges on resorption surfaces with large jumps (up to 30%) in An mol % content. The compositions of both resorbed and unresorbed phenocryst cores have a bimodal distribution with compositions of $An_{55–60}$ and $An_{75–90}$. Approximately half of the calcic intermediary zones are resorbed and a significant proportion of

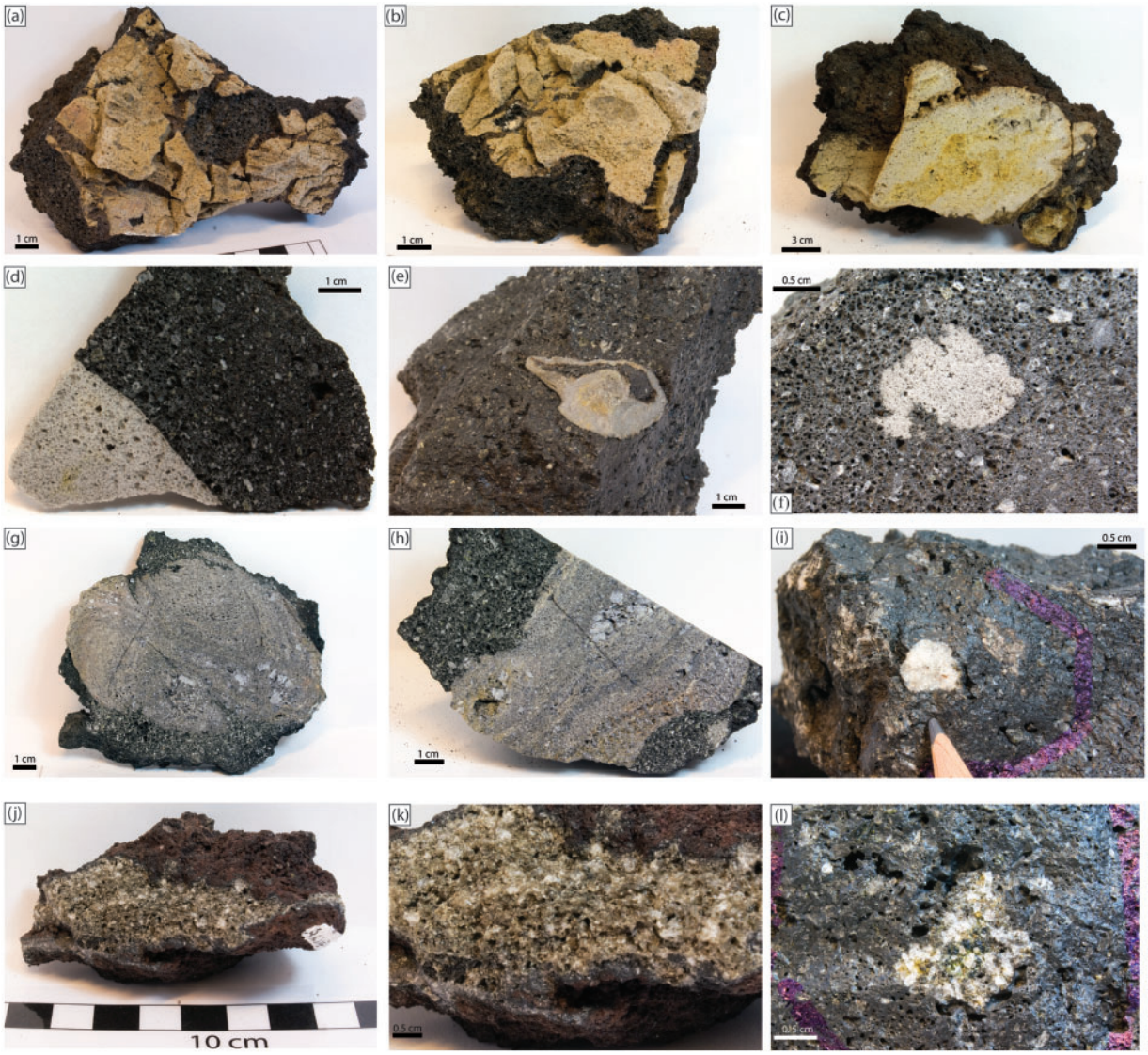

Fig. 2. Types of common xenolith in Anak Krakatau lavas. (a–c) Fragments of larger cream to grey-coloured, frothy, metapelitic xenoliths ('xeno-pumices') that are common in Anak products. (d–f) Small-scale features of frothy metasedimentary xenoliths. (Note the ductile shape of some smaller xenolith fragments, pointing towards xenolith disintegration in a hot and plastic state.) (g, h) Banded frothy xenolith with plastic deformation features (e.g. folding) and larger aggregates of pyro-metamorphic minerals such as cordierite [e.g. in (h), just top right of centre]. (i) Isolated cordierite xenocryst in Anak lava, testifying to the complete disintegration of some xenoliths. (j, k) Crystalline xenolith with frothy texture and glassy margin, probably of dioritic provenance, that is intensely strung out; (k) is close-up view of (j). (l) Small fragment of gabbroic composition in Anak lava.

Table 3: Modal analyses of representative polished thin sections

Sample	Plag.	Opx.	Cpx.	G'mass	Oxides	Glass	Xenos	Apatite
AK.LF	25·7	1·5	4·0	58·7	3·8	3·3	0·4	2·6
AK.XIc-11	35·6	1·4	6·1	47·0	5·6	2·7	0·0	1·6
AK1	33·4	4·6	3·5	50·1	6·8	1·3	0·2	0·0
K.CS-2	34·5	6·4	3·2	43·2	5·4	1·8	5·0	0·4
K.L-01	35·7	6·8	3·3	44·5	6·6	2·3	0·8	0·2

A total of 1000 points were counted and recalculated to a vesicle-free basis. Plag, plagioclase; Opx, orthopyroxene; Cpx, clinopyroxene; G'mass, groundmass; Xenos, xenolithic material.

phenocrysts have sodic cores that are of similar composition to the typical outer rims. Unresorbed intermediary zones are characterized by calcic plagioclase compositions ($An_{75–90}$), sieve-textured rims of slightly more sodic ($An_{65–85}$), and typical outer crystal rims are $An_{\sim 55–60}$ (Fig. 3b). Pyroxene phenocrysts do not display significant intra-crystal disequilibrium textures, yet rounding of their outer rims is common, suggesting disequilibrium with the final melt immediately prior to eruption.

The petrography, geochemistry and mineral chemistry of the 1883 Krakatau rhyodacitic pumices and obsidians have been described in detail by Mandeville *et al.* (1996) and will only be summarized briefly here. The phenocryst assemblage is dominated by clear, weakly zoned, euhedral to subhedral plagioclase and orthopyroxene, titanomagnetite, clinopyroxene, ilmenite, apatite and pyrrhotite (in order of decreasing abundance). Titanomagnetite, ilmenite, acicular apatite, and pyrrhotite frequently occur as inclusions within the plagioclase and pyroxene phenocryst phases. Glomerocrysts of plagioclase, pyroxene, glass and oxides can form 2–3 mm clots in both the pumice and obsidian. Irregular cognate lithic fragments and/or chilled mafic inclusions are also present in the deposit (Mandeville *et al.*, 1996; this study).

The diversity in the 2002 plagioclase compositions, most clearly shown amongst the core compositions, contrasts with the single population of $An_{45–55}$ phenocrysts reported from the 1883 white rhyodacites (Camus *et al.*, 1987; Mandeville *et al.*, 1996), but shows a strong similarity to phenocryst populations from the 1981 andesitic eruption of Anak Krakatau ($An_{40–55}$ and $An_{75–90}$; Camus *et al.*, 1987). In the grey dacitic 1883 pumices, equal proportions of reversely and normally zoned plagioclase are recorded, with rim compositions slightly more calcic than in the white rhyodacites at An_{52} and with rare core compositions of $An_{\sim 80}$ (Mandeville *et al.*, 1996).

The xenoliths from within the 2002 basaltic andesite samples vary considerably in composition, comprising

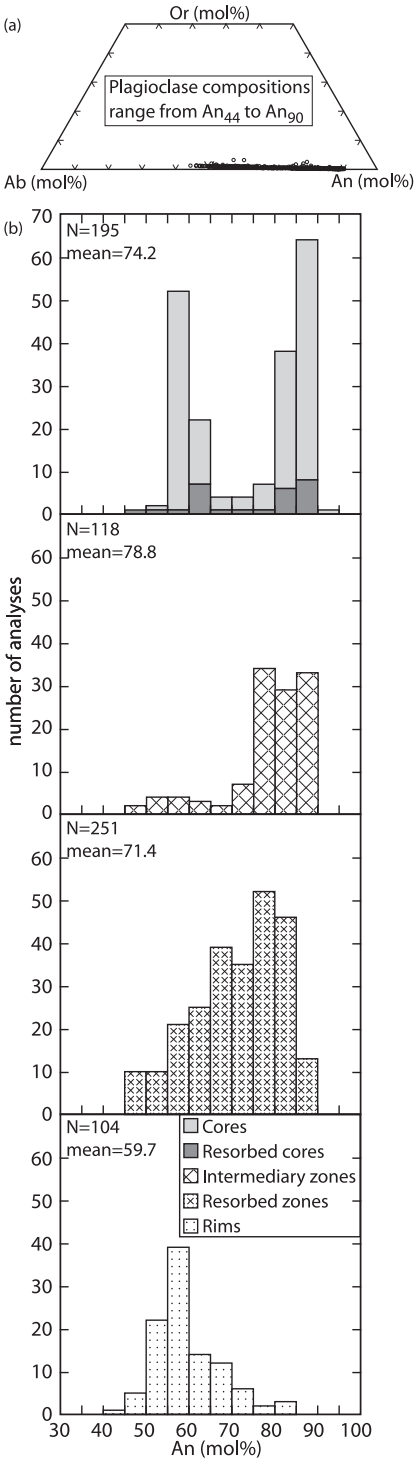

Fig. 3. (a) An–Ab–Or triangular plot (for Or = 0–50% only) showing all plagioclase analyses from Anak Krakatau basaltic andesites. Compositions range from An_{44} to An_{90} ($n = 668$). (b) Histograms of EMP analyses showing compositional variation amongst plagioclase phenocrysts in basaltic andesite from the 2002 eruption. Cores, rims and intermediary zones were identified from BSE images, and binned compositions were plotted on separate histograms for correlation. (Note the bimodal distribution for plagioclase core compositions, and the unimodal lower An content of the crystal rims.)

gabbroic rocks, aphanitic felsic compositions and relatively abundant frothy-textured metasediments (Fig. 2). Chemical equilibrium with the host magma has not been fully achieved in most cases and variable degrees of thermal overprinting and partial melting are recorded. A significant proportion of the xenoliths also contain high-temperature (pyro)-metamorphic minerals. For example, mineral assemblages observed in the frothy silicic metasedimentary xenoliths comprise cordierite + tridymite + anorthoclase + albite ± hornblende (identified by XRD analysis) (Table 4, Fig. 2a–i). Many of these xenoliths have also deformed in a ductile manner as they were incorporated into the basaltic andesite, producing folded and elongate anatectic textures (e.g. Fig. 2f–k). For example, sample AK.Xlf-04 from the 2001–2002 eruption is an elongated and frothy xenolith of crystalline material (probably from a dioritic protolith), where polycrystalline quartz (a re-equilibration texture) is apparently 'smeared' alongside a glassy, feldspar-phyric pumice-like interior (Fig. 2j and k).

Cordierite, common in the silicic metasedimentary xenoliths of our sample set (Fig. 2a–i), has previously been identified in 'pumice bombs' from the earliest activity of Anak Krakatau; Stehn (1929) reported white glassy '1883 pumice-like' masses encrusted in darker blackish brown to black porous basaltic andesite. The cores of these 'pumice bombs' contain numerous, fine to several milimetre-sized, idiomorphic crystals of cordierite, which show unusually high pleochroism. These xenoliths are identical to what were subsequently identified as 'frothy metasedimentary xenoliths' in the younger Anak Krakatau deposits (e.g. Mandeville *et al.* 1996; Fig. 2) and bear a certain resemblance to what was recently termed 'xeno-pumice' in the most recent El Hierro eruption in the Canary Islands (i.e. pumice-like texture but xenolithic in origin; Troll *et al.* 2012). In addition, XRD analysis was carried out on two fine-grained non-vesicular lithic clasts from the 1883 deposits. Sample K.S.SC-01, a siliciclastic sedimentary sample, is composed simply of quartz and albite, whereas sample K.S.SC-05, a mudstone, contains dolomite, muscovite and microcline (Table 4).

Dioritic to granitic xenoliths and a small number of olivine-bearing gabbro xenoliths (Fig. 2j–l) were also recovered from the 2002 basaltic andesites and are considered to represent mid- to lower-crustal cumulate assemblages from beneath the Krakatau volcanic complex. The 0·5–2 cm diorite fragments consist of plagioclase, clinopyroxene and orthopyroxene, and are notably less abundant than the metasedimentary xenoliths. However, small gabbroic and dioritic xenoliths (up to 5 mm) are common in many samples from Anak Krakatau, indicating a considerable degree of incorporation of this material (Fig. 2l). Granitic clasts from the Krakatau deposits were previously reported by Oba *et al.* (1982, 1992), and are composed of quartz, plagioclase, potassium feldspar, chloritized biotite pseudomorphs, occasional hornblende and opaque minerals, with accessory apatite. These xenoliths provide an additional source of information on the crustal lithologies underlying the volcanic complex.

Whole-rock geochemistry

Whole-rock major and trace element data for representative samples are reported in Table 5 (normalized to 100% volatile free); the complete set of analytical data is available as Supplementary Data in Electronic Appendix 1 (all Electronic Appendices can be downloaded from http://www.petrology.oxfordjournals.org).

Anak Krakatau samples from the 2002 eruption (Fig. 4a–d) plot within a narrow range from 54 to 56 wt % SiO_2, and are classified as basaltic andesites (filled diamonds). Our analyses of the 1883 products span a range from andesite to rhyolite (62–75 wt % SiO_2; large filled circles) and support the hypothesis that the 1883 olive obsidians are the quenched equivalents of the white rhyodacitic pumices (small open circles; data from Mandeville *et al.*, 1996).

Xenoliths span a large range of compositions (24–70 wt % SiO_2). The frothy metasedimentary xenoliths from within the young basaltic andesites predominantly plot

Table 4: XRD analysis of representative samples

Sample name	Sample type	Mineralogy
AK.Xla-05	Anak Krakatau lava	albite, augite, anorthoclase
AK.Xlf-02	frothy metasedimentary xenolith	albite, anorthoclase
AK.Xlf-15	frothy metasedimentary xenolith	cordierite, hornblende, quartz, albite
AK.Xlf-27	frothy metasedimentary xenolith	cordierite, quartz
AK.Xlf-32	frothy metasedimentary xenolith	cordierite, tridymite, anorthoclase, albite
K.S.SC-01	lithic clast in 1883 deposits	quartz, albite
K.S.SC-05	lithic clast in 1883 deposits	dolomite, muscovite, microcline

Table 5: Representative major and trace element analyses of whole-rock samples from the Krakatau volcanic complex and surrounding crust

Group:	Anak	Anak	Anak	Anak	1883	1883	1883
Sample:	AK-1	AK.Xlc-03	AK.Xla-05	AK.Xlc-11	K.P.WP-01	K.S.Ob-01	K.S.P-03
wt %							
SiO_2	55·71	55·54	54·89	54·45	68·52	67·98	62·79
TiO_2	1·06	1·09	1·11	1·11	0·65	0·68	1·00
Al_2O_3	17·92	17·80	17·66	18·01	14·41	14·44	16·07
FeO*	8·07	8·28	8·74	8·52	3·08	5·89	5·40
MnO	0·17	0·18	0·18	0·18	0·12	0·12	0·14
MgO	4·04	4·04	4·30	4·35	1·37	0·95	2·05
CaO	8·31	8·11	8·39	8·63	2·57	2·59	5·08
Na_2O	3·50	3·66	3·49	3·53	6·75	4·95	5·51
K_2O	0·94	0·98	0·93	0·92	2·40	2·25	1·65
P_2O_5	0·27	0·32	0·32	0·31	0·14	0·15	0·29
Trace elements analysed by XRF (ppm)							
V	197	213	225	215	30	42	69
Cr	30	238	47	266	b.d.	b.d.	b.d.
Co	b.d.	26.	79	26	22	32	b.d.
Ni	13	570	15	616	b.d.	b.d.	1
Zn	72	76	76	74	64	69	62.
Ga	b.d.	16	15	17	14	13	b.d.
Rb	23	26	25	21	60	65	43
Sr	383	367	371	376	189	194	284
Y	33	33	28	32	50	53	44
Zr	123	129	122	116	272	278	188
Nb	4	5	7	6	11	13	6
Ba	181	194	177	173	372	374	244
Trace elements analysed by ICP-MS (ppm)							
La	15·019	14·786	14·469	14·239	24·800	27·575	20·934
Ce	35·423	35·039	34·645	33·484	57·236	64·279	49·225
Pr	4·781	4·700	4·689	4·502	7·565	8·385	6·608
Nd	21·511	21·330	20·738	20·254	31·704	35·837	29·088
Sm	5·294	5·196	5·101	4·876	7·454	8·451	6·952
Eu	1·528	1·496	1·488	1·456	1·712	1·911	1·833
Gd	5·398	5·469	5·226	5·145	7·689	8·680	7·140
Tb	0·865	0·851	0·838	0·825	1·245	1·395	1·169
Dy	5·408	5·360	5·161	5·049	7·956	9·025	7·341
Ho	1·106	1·106	1·089	1·048	1·672	1·855	1·485
Er	3·261	3·292	3·202	3·117	5·127	5·652	4·589
Tm	0·509	0·521	0·502	0·483	0·825	0·940	0·714
Yb	3·057	3·118	3·131	2·955	5·247	5·884	4·494
Lu	0·494	0·486	0·479	0·464	0·810	0·905	0·692
Hf	3·105	3·260	2·951	3·128	6·287	7·035	4·935
Ta	1·059	0·247	2·031	0·214	0·684	1·483	0·330
Pb	4·492	5·658	5·265	5·214	11·139	13·062	8·806
Th	3·034	3·275	2·987	2·935	7·579	8·274	5·435
U	0·739	0·789	0·737	0·720	1·803	1·993	1·323

(continued)

Table 5: Continued

Group:	Pre-1883	Crust	Crust	Crust	Xenolith	Xenolith	Xenolith	Xenolith
Sample:	K.S.IC-03	K.S.SC-05	K.S.SC-06	K.S.SC-07	AK.Xlf-15	AK.Xlf-23	AK.Xlf-27	AK.Xla-05 x
wt %								
SiO_2	62·01	24·42	23·15	72·92	63·30	68·56	64·50	50·22
TiO_2	0·98	0·43	0·40	0·63	1·02	0·80	1·03	1·02
Al_2O_3	17·05	9·02	8·60	13·57	21·56	15·31	20·98	22·94
FeO*	5·92	2·62	2·46	3·25	6·69	3·95	6·56	9·87
MnO	0·14	0·37	0·24	0·09	0·14	0·10	0·05	0·09
MgO	1·97	25·95	26·39	1·86	2·47	1·11	1·67	2·21
CaO	5·64	35·71	37·37	1·36	0·85	3·54	0·81	9·57
Na_2O	4·26	0·33	0·27	3·70	0·95	4·94	1·89	3·38
K_2O	1·71	0·72	0·66	2·52	2·87	1·50	2·38	0·48
P_2O_5	0·33	0·43	0·45	0·11	0·15	0·18	0·11	0·21
Trace elements analysed by XRF (ppm)								
V	123	35	38	47	174	33	138	170
Cr	b.d.	26	22	19	90	b.d.	67	13
Co	34	23	28	9	105	22	43	b.d.
Ni	b.d.	7	8	b.d.	53	10	52	28
Zn	68	23	20	65	113	46	b.d.	64
Ga	16	b.d.	b.d.	15	21	16	19	168
Rb	48	27	24	64	158	41	84	10
Sr	298	443	438	135	126	271	81	499
Y	41	7	12	38	22	50	26	33
Zr	209	48	46	182	168	239	220	219
Nb	9	3	5	10	17	11	17	6
Ba	268	40	49	302	344	298	289	135
Trace elements analysed by ICP-MS (ppm)								
La	21·893	10·457	8·742	19·839	30·375	22·337	39·564	21·089
Ce	51·748	21·481	18·083	44·963	63·378	52·786	87·512	44·893
Pr	6·833	2·353	1·972	5·746	7·386	6·974	10·016	5·507
Nd	29·704	7·781	7·551	23·252	28·014	30·472	38·406	22·687
Sm	7·187	1·675	1·485	5·569	5·604	7·376	7·593	5·167
Eu	1·802	0·357	0·315	1·423	1·171	1·930	0·857	1·851
Gd	7·399	1·385	1·275	5·876	4·931	7·864	6·550	5·337
Tb	1·194	0·218	0·192	0·949	0·775	1·292	1·038	0·910
Dy	7·508	1·168	1·070	6·275	4·511	8·344	6·103	5·772
Ho	1·527	0·233	0·214	1·307	0·886	1·730	1·208	1·245
Er	4·523	0·660	0·602	4·021	2·553	5·230	3·379	3·793
Tm	0·737	0·108	0·102	0·671	0·396	0·834	0·536	0·619
Yb	4·496	0·658	0·615	4·132	2·466	5·259	3·257	4·075
Lu	0·704	0·097	0·095	0·650	0·363	0·815	0·481	0·626
Hf	5·502	0·904	0·942	4·474	3·133	5·551	2·816	6·370
Ta	1·262	0·267	0·267	0·356	4·297	1·009	1·014	0·506
Pb	9·044	6·718	6·364	10·775	30·309	8·569	1·219	3·467
Th	6·328	4·142	3·656	6·175	14·009	6·336	17·392	10·690
U	0·479	1·235	1·109	1·515	3·237	1·516	2·301	2·457

All data normalized to 100% volatile-free. b.d., below detection limit.
*Total iron as FeO.

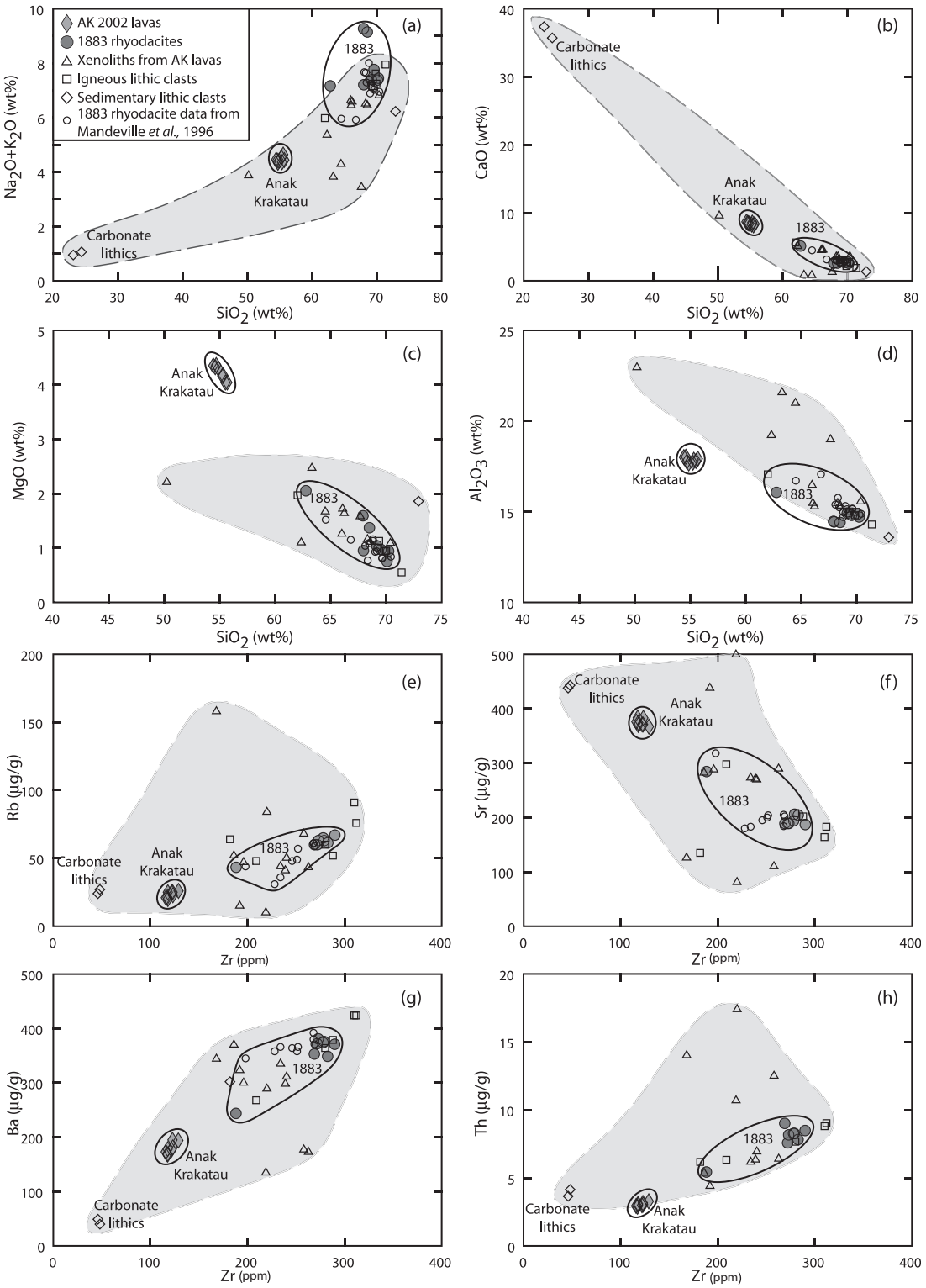

Fig. 4. Major and trace element variations for Anak Krakatau, 1883 and related samples. Major oxides are plotted against SiO_2 (concentrations in wt %) and trace elements against Zr (in ppm). Xenoliths (e.g. metasedimentary and igneous clasts) are also shown [note the different scale in (c) and (d) when the carbonate lithics are not plotted]. Data from Mandeville *et al.* (1996) are also included as small open circles. The fields outlined with dashed and continuous lines denote the range of Anak Krakatau basaltic andesites and in the composition of the 1883 eruption products, respectively. The grey field defines the entire range of possible contaminants, defined by lithic clasts from within the 1883 deposits and xenoliths from the Anak Krakatau lavas.

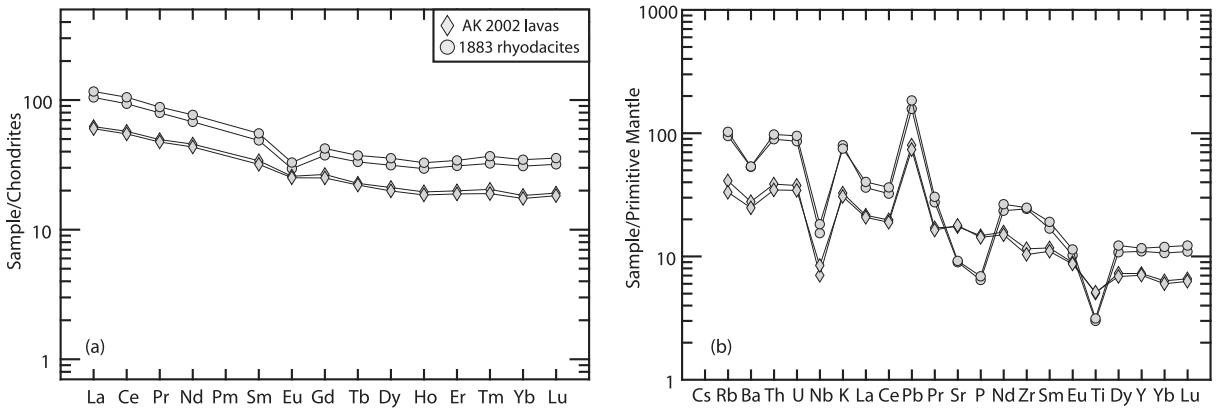

Fig. 5. (a) Rare earth element patterns showing the extent of variation within the Anak Krakatau 2002 (AK.Xlc-03 and AK.Xlc-11) and the 1883 Krakatau samples (K.S.Ob-01 and K.P.WP-01). Data normalized to chondrite (Sun & McDonough, 1989). (b) Extended incompatible trace element plots normalized to primitive mantle (Sun & McDonough, 1989). (Note the negative Eu anomaly in both the Anak and 1883 products.)

Table 6: Representative Nd–Sr-O isotopic data for whole-rock samples from the Krakatau volcanic complex and surrounding crust

Group	Sample	$^{87}Sr/^{86}Sr$	Error (2SD)	$^{143}Nd/^{144}Nd$ (2SD)	Error	$\delta^{18}O$
Anak	AK-1	0·704417	±16	0·512779	±7	—
Anak	AK.Xlc-03	0·704419	±15	0·512801	±14	6·3
Anak	AK.Xla-05	0·704381	±9	0·512793	±7	6·7
Anak	AK.Xlc-11	0·704515	±14	0·512783	±13	6·4
1883	K.P.WP-01	0·704670	±9	0·512793	±7	8·0
1883	K.S.Ob-01	0·704420	±13	0·512778	±14	7·3
1883	K.S.P-03	0·704541	±14	0·512810	±7	—
Pre-1883	K.S.IC-03	0·704405	±6	0·512791	±6	6·5
Crust	K.S.SC-05	0·709140	±14	0·512790	±7	—
Crust	K.S.SC-06	0·709130	±6	—	—	25·5
Crust	K.S.SC-07	0·707133	±15	0·512769	±6	—
Xenolith	AK.Xlf-15	—	—	0·512211	±7	13·6
Xenolith	AK.Xlf-23	0·704488	±7	0·512812	±6	3·2
Xenolith	AK.Xlf-27	0·708720	±6	0·512425	±6	5·5
Xenolith	AK.Xla-05 x	0·704659	±18	0·512669	±6	8·2

Values in italics denote radiogenic isotope ratios from WSU; all others from SUERC. Oxygen isotope data are from University of Cape Town. Errors are last relevant digits.

intermediate between the 1883 Krakatau eruptive products and the Anak lavas, but the suite also includes more mafic gabbroic xenoliths (e.g. sample AK.Xla-05 x, ~50 wt % SiO_2 and ~10 wt % CaO; see Fig. 4). Igneous lithic clasts (open squares) from within the 1883 deposits also probably represent a 'pre-1883' Krakatau component and display very similar compositions to the 1883 rhyodacites (this study and Mandeville *et al.*, 1996). The rare carbonate-rich sedimentary clasts are compositionally distinct, with ~36 wt % CaO and ~24 wt % SiO_2 (small open diamonds).

Abundances of Rb, Ba and Th in the Anak Krakatau lavas and 1883 rhyodacites define a broadly positive correlation with increasing Zr, whereas Sr is negatively correlated (Fig. 4e–h). The xenolith population from the Anak lavas, along with the variety of lithic fragments in the

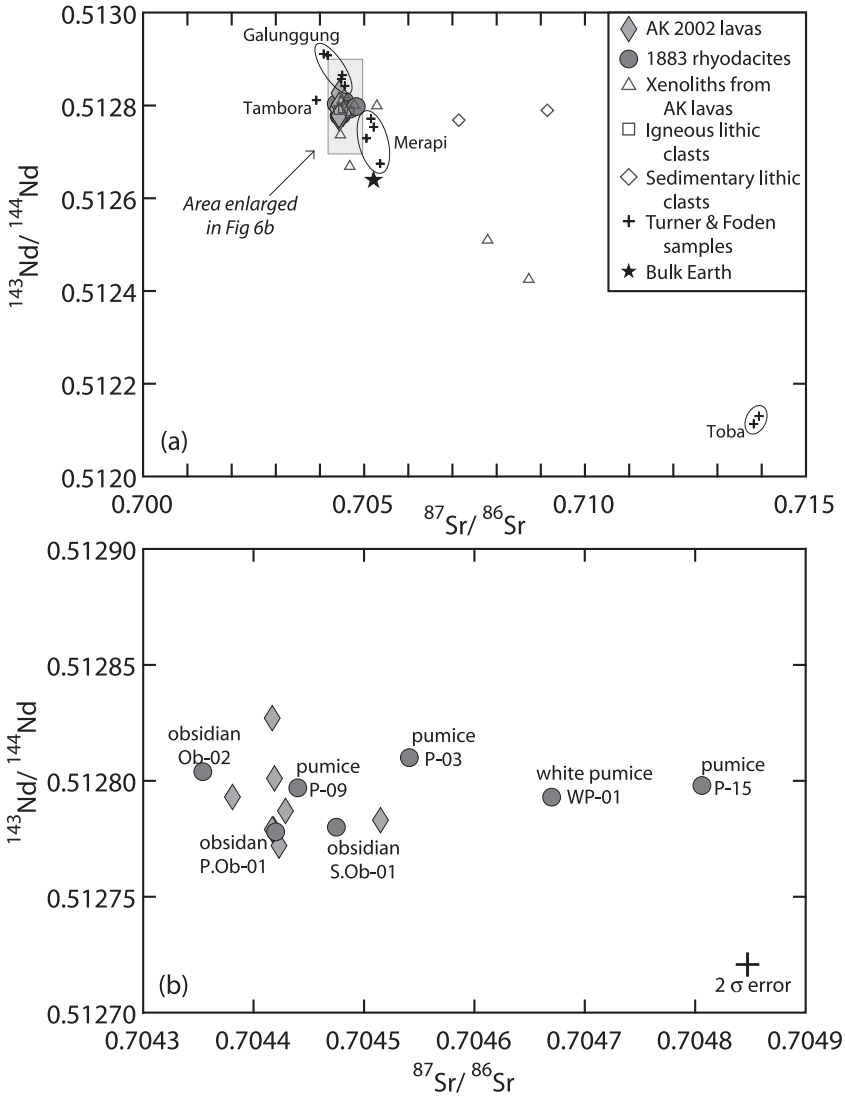

Fig. 6. $^{143}Nd/^{144}Nd$ vs $^{87}Sr/^{86}Sr$ variation diagrams for (a) whole-rock analyses from the Krakatau complex and other Sunda Arc volcanoes: Toba, Galunggung, Merapi and Tambora; data from Turner & Foden, 2001) and (b) enlarged diagram showing Krakatau samples only. A trend towards more radiogenic $^{87}Sr/^{86}Sr$ values from Anak Krakatau basaltic andesites to the 1883 rhyodacites with limited variation in $^{143}Nd/^{144}Nd$ is observed. (See Table 6 and Electronic Appendix 1 for further data for the labelled 1883 samples.)

1883 deposits, can be regarded as possible contaminants of the Krakatau magmatic system and therefore this range is highlighted by the grey shaded fields in Fig. 4a–h.

Chondrite-normalized REE patterns for the Anak and 1883 samples are virtually parallel, showing a greater negative Eu anomaly in the more evolved 1883 products (Eu/Eu* = 0·68 in comparison with 0·87 for Anak) (Fig. 5). Light REE (LREE) are moderately enriched relative to the MREE [$(Ce/Sm)_n$ ~1·6 for Anak and ~1·8 for 1883], with the heavy REE (HREE) being essentially unfractionated [$(Dy/Lu)_n$ ~1·1 for Anak and 1·0 for 1883]. Notably, there is limited variation between samples of Anak Krakatau lavas and 1883 rhyodacites (Fig. 5a). Primitive mantle normalized incompatible trace element patterns (Fig. 5b) show typical volcanic-arc signatures with depletion of Nb relative to La, enrichment of Pb relative to Ce, higher abundances of large ion lithophile elements (LILE; e.g. K, Rb, Ba) and deficiencies of high field strength elements (HFSE; e.g. Nb, Ta, Ti). The diagram uses data from K.S.Ob-01 and K.P.WP-01 to show the range in 1883 compositions, and AK.Xlc-03 and AK.Xlc-11 to show the variation in Anak products. Samples K.S.Ob-01 and AK.Xlc-11 represent the boundaries for the entire 1883 to Anak field.

Measured whole-rock $^{87}Sr/^{86}Sr$ and $^{143}Nd/^{144}Nd$ values are similar to those of other stratovolcanoes in the Sunda arc (e.g. Galunggung, Tambora, Merapi; Turner & Foden, 2001; Table 6 and Electronic Appendix 1). Anak Krakatau

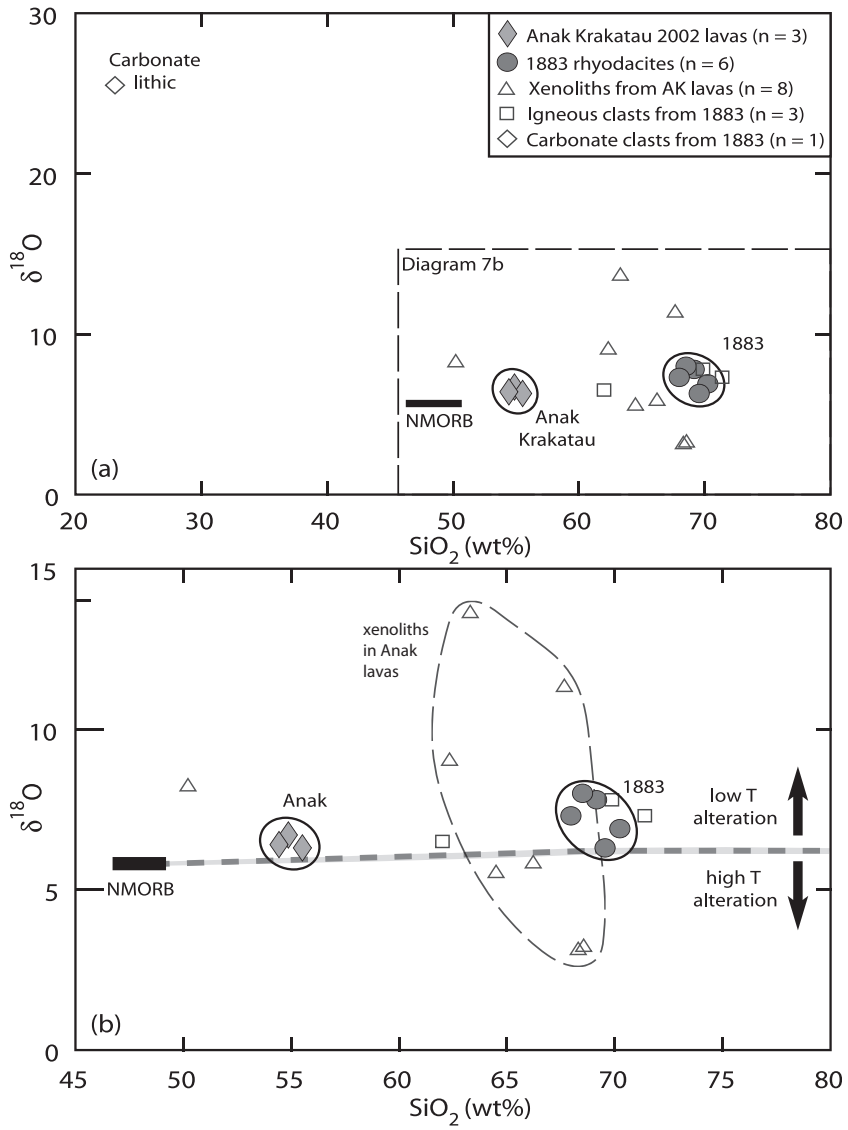

Fig. 7. Variation of $\delta^{18}O$ in whole-rocks from the Krakatau Volcanic complex as a function of silica content: (a) SiO_2 from 20 to 80 wt %, with dashed-line box depicting the enlarged area shown in (b) (SiO_2 from 45 to 80 wt %). The 1883 eruptive rocks and Anak Krakatau samples plot above to a magmatic differentiation trend from normal mid-ocean ridge basalt (N-MORB) and the xenolith samples show evidence of both low- and high-temperature hydrothermal overprints. The grey dashed line indicates Rayleigh fractionation of $\delta^{18}O$ values, with an approximate 0·2‰ change per 5% rise in SiO_2 content expected for closed-system fractionation of felsic magmas (after Taylor & Sheppard, 1986; Bindeman *et al.*, 2004).

$^{87}Sr/^{86}Sr$ ranges range from 0·704381 to 0·704515 and 1883 samples from 0·704354 to 0·704806. The variations are restricted compared with the range of the xenoliths observed and with the variations of other Sunda arc volcanoes such as Toba (Fig. 6a and b). A reported $^{87}Sr/^{86}Sr$ value of 0·70434 from a pre-1883 andesitic lava flow from Panjang (Whitford, 1975) is somewhat lower, but essentially within analytical error of our data.

Bulk-rock $\delta^{18}O$ values of the basaltic andesites (6·3–6·7‰) span a much narrower range than those of the 1883 rhyodacites (6·2–7·8‰). Carbonate-rich sedimentary clasts from the 1883 deposits have the most extreme $\delta^{18}O$ values in the Krakatau vicinity (Fig. 7). Metasedimentary xenoliths from the Anak basaltic andesite lavas, in turn, demonstrate the largest $\delta^{18}O$ range, from 3·1 to 13·6‰. Strontium isotope ratios do not correlate with $\delta^{18}O$ values (not shown).

Plagioclase *in situ* analyses

Selected plagioclase phenocrysts from the Anak Krakatau basaltic andesites were analysed by EMP and by LA-ICP-MS for $^{87}Sr/^{86}Sr$ (Table 7 and Electronic Appendix 3).

Table 7: Representative LA-ICP-MS analyses of plagioclase phenocryst zoning

Analysis	Area of crystal	$^{87}Sr/^{86}Sr$	Error (2SD)
AK-1-pl-01			
P1	core	0·70434	±0·00007
P2	core	0·70437	±0·00005
P3	outer rim	0·70450	±0·00004
AK-1-pl-03			
P1	outer core	0·70441	±0·00006
P2	outer core	0·70435	±0·00006
P3	zone 1	0·70444	±0·00006
P4	zone 2	0·70463	±0·00009
P5	inner core	0·70439	±0·00007
P6	zone 2	0·70482	±0·00007
P7	outer rim	0·70482	±0·00008
P8	outer rim	0·70442	±0·00006
P9	zone 2	0·70474	±0·00008
P10	outer rim	0·70461	±0·00007
P11	just inside outer rim	0·70484	±0·00010
AK-1-pl-04			
P1	outer core	0·70431	±0·00006
P2	inner core	0·70447	±0·00007
P3	zone 2	0·70475	±0·00006
P4	outer rim	0·70443	±0·00005
P5	zone 1	0·70454	±0·00005
P6	zone 2	0·70452	±0·00008
P7	outer core	0·70453	±0·00009
P8	inner core	0·70437	±0·00005
P9	zone 1	0·70437	±0·00005
P10	outermost rim	0·70454	±0·00006
AK-1-pl-09			
P1	outer rim	0·70444	±0·00004
P2	broad zone	0·70441	±0·00005
P3	inner dark grey zone	0·70445	±0·00005
P4	inner dirty zone	0·70443	±0·00006
P5	outer rim	0·70434	±0·00005
P6	light grey zone	0·70434	±0·00005
P7	dark grey zone	0·70452	±0·00005
P8	light grey dirty interior	0·70446	±0·00006
P9	light grey zone	0·70439	±0·00005
P10	dark grey zone	0·70464	±0·00005
G'mass 1	small crystal	0·70441	±0·00005
G'mass 2	small crystal	0·70444	±0·00007
G'mass 3	medium crystal	0·70444	±0·00004
G'mass 4	medium crystal	0·70446	±0·00005
G'mass 5	euhedral	0·70431	±0·00006

See Fig. 8a–d for locations of laser ablation pits and troughs.

Back-scattered electron (BSE) images of these plagioclase are shown in Figs 8 and 9 (Part I) alongside graphic representations demonstrating the cores, zoning and rims (Part II).

Crystal AK1-pl01 (Fig. 8a) has a calcic core, a broad sieve-textured, resorbed intermediary zone with an abundance of melt inclusions, and a narrow sodic rim. This is coupled with a small increase in radiogenic Sr towards the rim from ~0·70435 to 0·70450 (see Table 7 for calculated error values).

Crystal AK1-pl03 (Fig. 8b) is the largest analysed phenocryst (5 mm in diameter) and shows a resorbed calcic core, a very broad sieve-textured overgrowth zone with an abundance of melt inclusions, and a narrow sodic rim. A low $^{87}Sr/^{86}Sr$ value of 0·70435 in the core rises sharply to 0·70463 and 0·70474. A value of 0·70482 in the outer rim is in clear disequilibrium with the surrounding melt (0·70440, estimated from analyses of micro-phenocrysts, or 0·704417 from whole-rock analyses).

Crystal AK1-pl04 (Fig. 8c) has an inner core of $An_{86–87}$ compared with an outer core of $An_{89–90}$, a sieve-textured overgrowth zone, and an oscillatory zoned narrow sodic outer rim. Radiogenic Sr isotope ratios initially decrease to an outer core of 0·70430 and then subsequently increase from the outer core towards the rim of 0·70450.

Crystal AK1-pl09 (Fig. 8d) has a large resorbed core rimmed by a wide calcic overgrowth zone, and a narrow sodic outer rim. Despite the significant variation in anorthite content of >30 mol % along the illustrated EMP traverse, $^{87}Sr/^{86}Sr$ remains consistently low at ~0·70445. However, seven other LA-ICP-MS analyses of this plagioclase (which are remote from the EMP traverse and are listed in Table 7) show a significant variation in strontium isotope ratios of up to 0·70464.

Plagioclase phenocrysts with more complex zonation are shown in Fig. 9. Crystal AK1-pl06 (Fig. 9a) has a highly variable anorthite content with a strongly resorbed core and non-systematic variations in $^{87}Sr/^{86}Sr$ (e.g. radiogenic core).

Crystal AK1-pl13 (Fig. 9b) has a resorbed core with abrupt fluctuations in anorthite content of >25 mol % and a severely sieve-textured intermediate zone with a thin (<0·05 mm) outer rim of $An_{\sim 75–85}$. Although the Sr isotope composition generally increases from core to rim, both high and low values of $^{87}Sr/^{86}Sr$ are recorded in plagioclase of $An_{\sim 57}$ and $An_{\sim 85}$. In the case of analysis AK1-pl13 P1 this is probably a depth effect, as the laser probably ablates through the core (shaded yellow) into the intermediary zone (shaded green), resulting in a value that is a mixture of the two zones.

Groundmass and microphenocryst plagioclase yielded low $^{87}Sr/^{86}Sr$ values of between 0·70431 and 0·70446 for medium-size microphenocrysts and 0·70440 for small microphenocrysts (see Table 7).

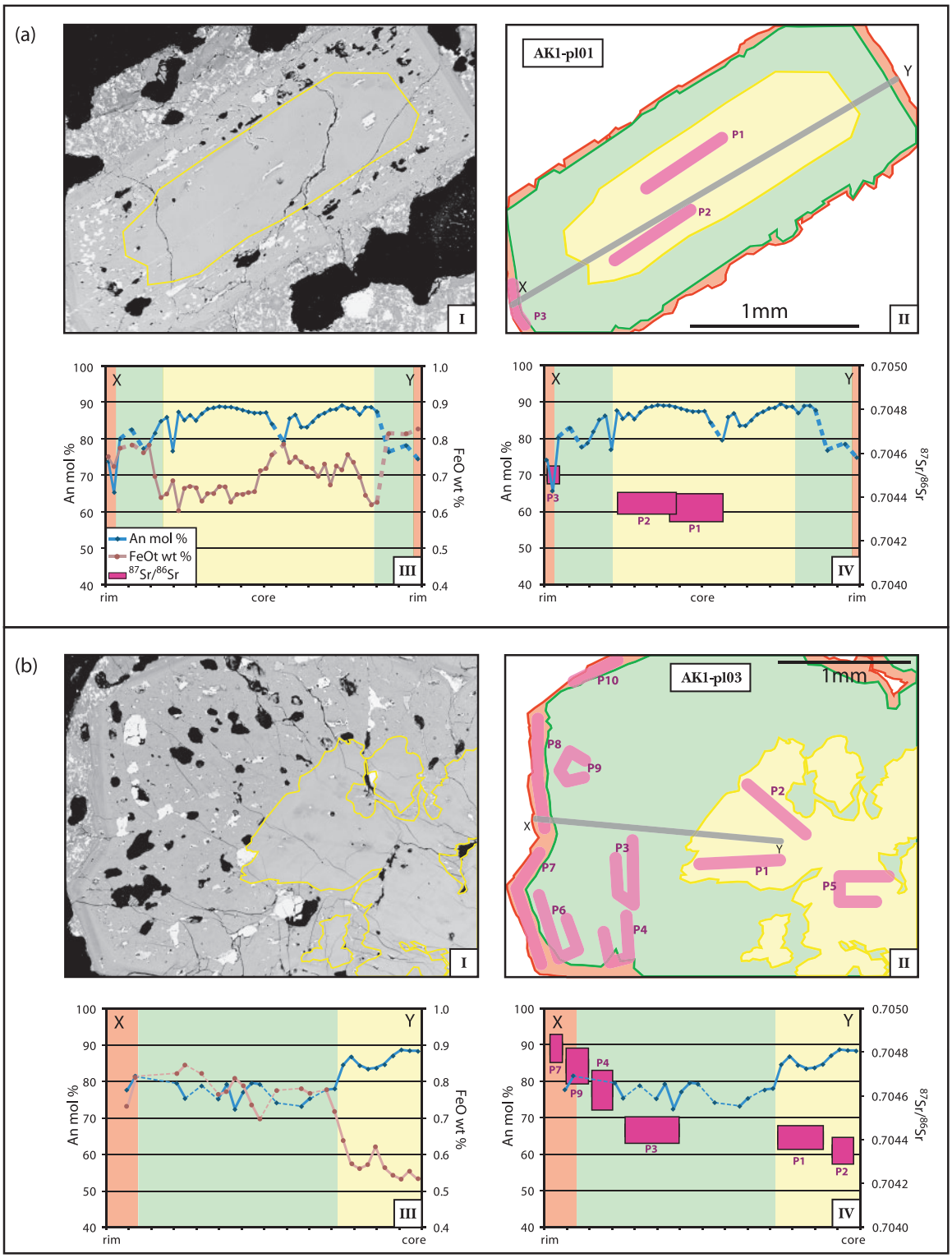

Fig. 8. Examples of plagioclase crystals broadly indicating AFC-type processes: (a) phenocryst AK1-pl01; (b) phenocryst AK1-pl03; (c) phenocryst AK1-pl04; (d) phenocryst AK1-pl09. Each section of (a)–(d) is split into four parts: part I, a back-scattered electron image to illustrate the plagioclase troughs; part II, a graphic representation of the plagioclase zones and the position of the $^{87}Sr/^{86}Sr$ LA-ICP-MS analyses and the EMP traverse (labelled X–Y); part III, An mol % (diamonds) and FeO_t wt % (circles) zoning profile from X to Y; part IV, An mol % profile plotted against $^{87}Sr/^{86}Sr$ (bars). In part IV, the length and height of the rectangles corresponds to the lasered area and analytical error (2SD), respectively.

(continued)

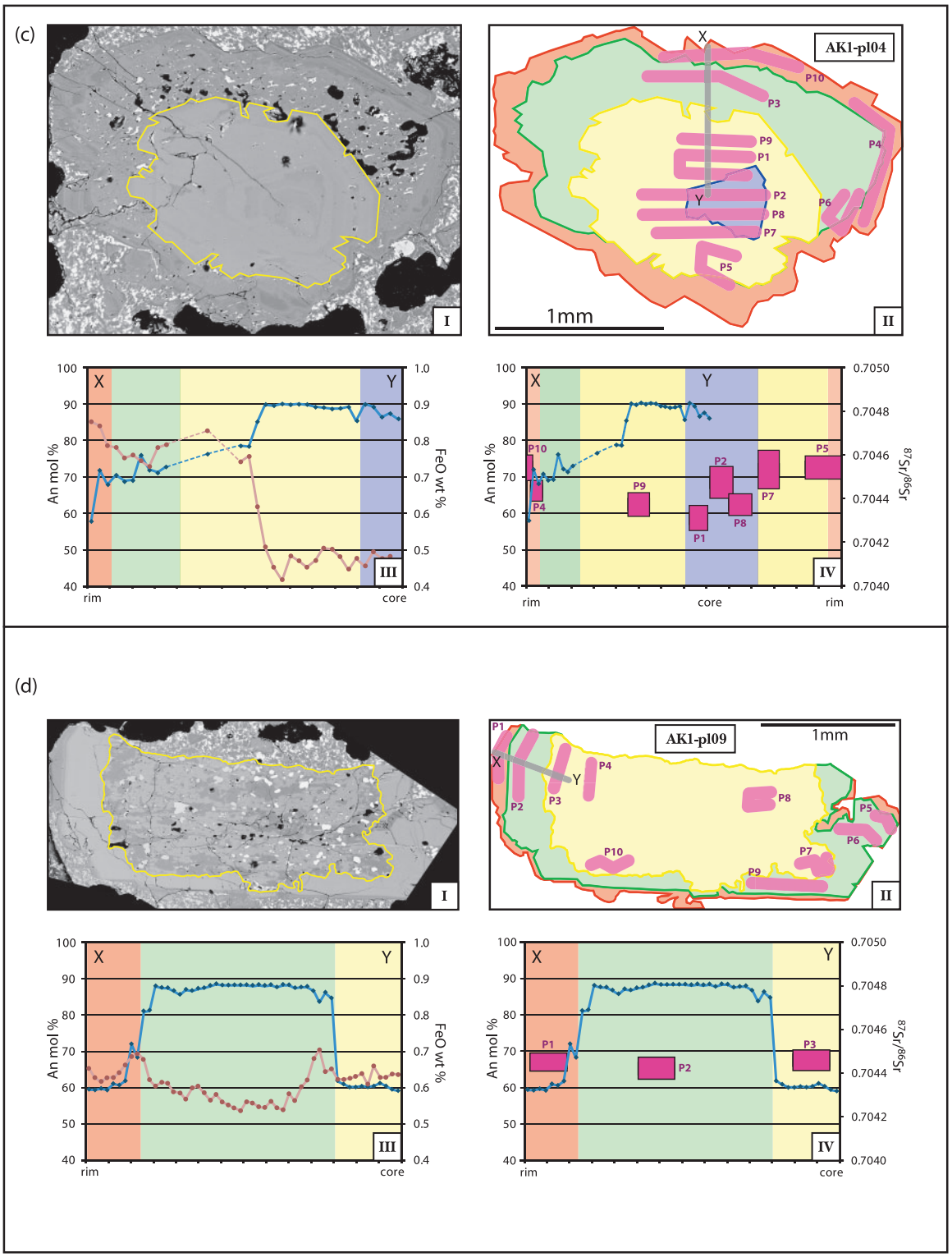

Fig. 8. Continued.

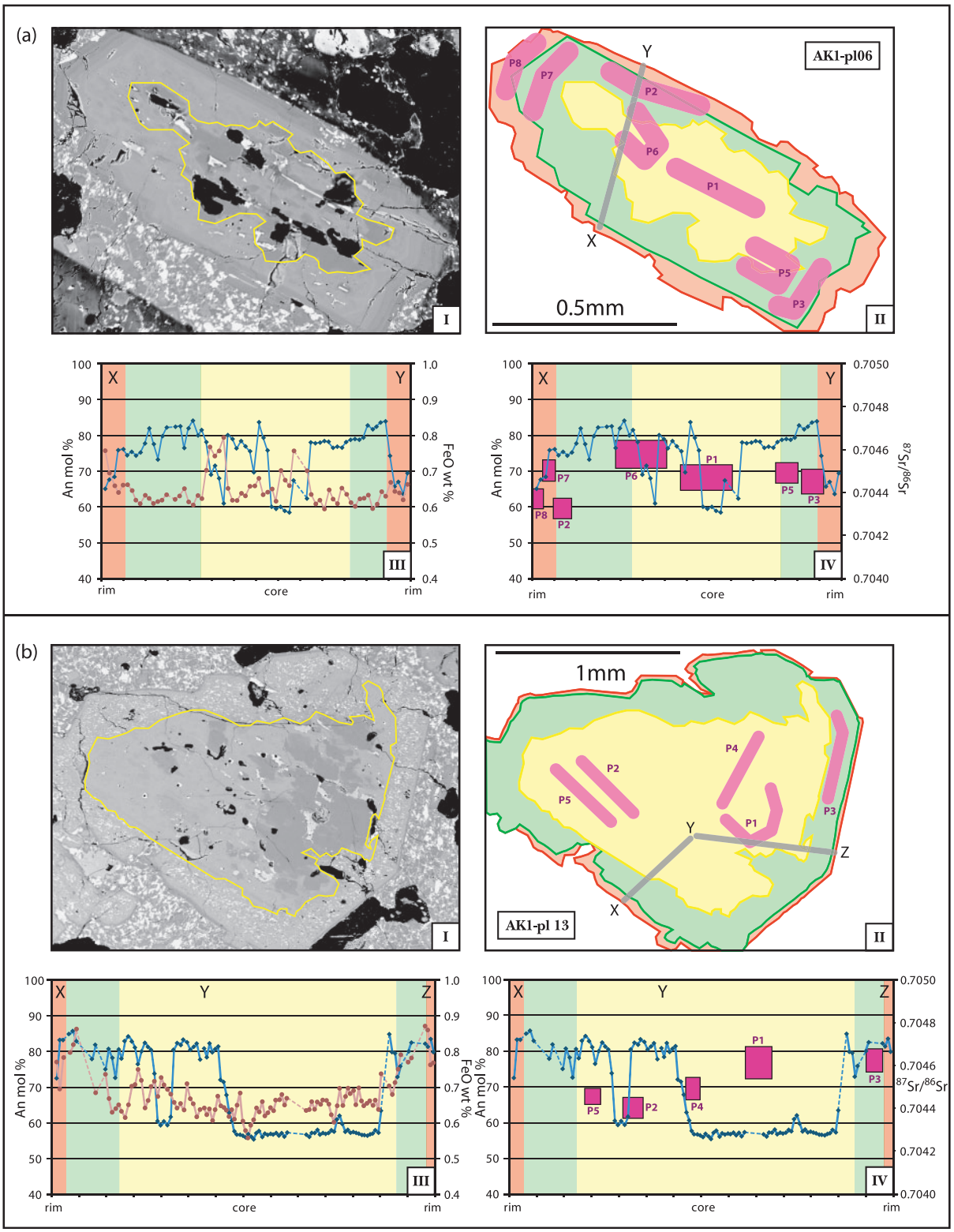

Fig. 9. Examples of plagioclase crystals showing complex zonation: (a) phenocryst AK1-pl06; (b) phenocryst AK1-pl 13. Descriptions for sections I–IV are given in Fig. 8 caption. [Note the different scale bar in (a), part II, highlighting the spatial limits of the LA-ICP-MS method.]

DISCUSSION

Petrology

Anak Krakatau lavas and 1883 rhyodacites

Phenocrysts from each stage of Krakatau's history display zoning textures that suggest progressively changing crystallization conditions that reveal *P*, *T*, *X* variations within the sub-volcanic complex, including low levels of assimilation.

All Krakatau products contain both plagioclase crystals that have high anorthite contents ($An_{75–85}$) and also more albitic ($An_{\sim 50–60}$) plagioclase crystals with a composition that is close to equilibrium with the host melt. In the 1883 grey dacite pumices the rare, highly calcic ($An_{\sim 80}$) plagioclase crystal cores (Mandeville *et al.*, 1996) are interpreted as inherited plagioclase phenocrysts from an andesitic parent magma to the 1883 rhyodacites, or 'antecrysts' recycled from cumulate material deeper in the volcanic system. The $An_{75–90}$ phenocrysts not in equilibrium with the andesitic melt of the 1981 eruption have previously also been interpreted as xenocrysts or antecrysts by Camus *et al.* (1987).

The plagioclase phenocryst population in the 2002 basaltic andesites indicates a return to crystal assemblages similar to those between 1927 and 1981, suggesting that pockets of magma may exist in the shallow crust that allow small magma batches to evolve to andesitic compositions and erupt in small-volume events such as that of 1981. This proposition of multiple small magma pockets and chambers in the shallowest crust is corroborated by reduced travel speeds of seismic waves despite the lack of a large seismically detectable magma reservoir at shallow levels (e.g. within the top 6–7 km; Harjono *et al.*, 1989; Jaxybulatov *et al.*, 2011).

Crustal fragments in the 1883 ignimbrites

The lithic clasts found within the 1883 deposits on the islands of Sertung and Panjang comprise samples from the subjacent crust in the region. The range of immature siltstones and sandstones, containing foraminifera and benthic fauna, and rare carbonate mudstones, is identical to the shallow crustal stratigraphy reported from Well C-1-SX, *c.* 30 km SE of Anak Krakatau (Noujaim, 1976; see Fig. 1).

Significance of the xenolith assemblage

Cordierite in xenolithic material (Fig. 2) indicates low-pressure, high-temperature metamorphism of pelitic sediments and forms a common constituent of pyrometamorphosed clay-rich quartzo-feldspathic rocks in contact metamorphic aureoles (e.g. Weiss & Troll, 1989). Occurring at pressures of less than 2 kbar and over a wide range of temperatures from 450 to >800°C (Grapes, 2006), cordierite provides an approximate geobarometer for the depth of incorporation of pelitic xenoliths into basic igneous intrusions (Renzulli *et al.*, 2003). High-temperature laboratory experiments show that iron cordierite melts incongruently to mullite, tridymite and a liquid at ~1210°C (Deer *et al.*, 1992). Although mullite has not been identified in our samples, tridymite occurs with cordierite in a number of foamy metapelitic xenoliths within the recent Anak Krakatau products. The presence of cordierite in metasedimentary xenoliths and as xenocrysts in the Anak lavas thus documents the interaction of relatively shallow crustal materials in approximately the top 5–6 km of the crust with hot ascending Anak magmas. This 'macro-scale' contamination of the Anak magmas is likely to explain the very notable 'cordierite-bearing "pumice-like" bombs' erupted previously in 1928 (Stehn, 1929) and bears similarities to the processes inferred for the 2011 El Hierro eruption (see Troll *et al.*, 2012).

Significance of the crustal composition and structure

To characterize the magma plumbing system and the compositional range of crustal additions we consider the approach of Hamilton (1979) and Oba *et al.* (1992), in which the deep basement underlying the Krakatau complex was regarded as similar to the peraluminous granites that dominate the western magmatic belt of the Malaysia Peninsula (see Metcalfe, 2011). Although the granitic xenoliths found within the 1883 pumices contain hornblende and may therefore be metaluminous, the proximity of the Sundaland terrane boundary and the additional gabbro and diorite xenoliths found within the Anak lavas provide a more accurate representation of the nature of the crystalline basement below the Late Miocene strata of the Krakatau Basin. This is an important consideration for our energy-constrained assimilation–fractional crystallization (EC-AFC) modelling, as the sub-Krakatau basement seems to differ somewhat from regular Malaysia-type crust and a geochemically variable character has to be assumed (e.g. gabbro–diorite–granite).

It has been shown that upper crustal sedimentary xenoliths are unlikely to survive in mafic magma for extended periods of time, with partial melting, disaggregation and the liberation of xenocrysts occurring rapidly, at orders of magnitude faster than typical repose times for arc volcanoes (Beard *et al.*, 2005; Dungan, 2005). Therefore, while the contact aureole around the volcanic system must be sufficiently influential for the growth of cordierite and tridymite, the abundance of crustal sedimentary xenoliths present in the erupted Anak Krakatau magmas suggests that those observed in outcrop were incorporated only shortly prior to eruption (hours to days) and are probably associated with rapid magma ascent leading to explosive (strombolian) types of events.

Bulk-rock geochemistry

The 1883 eruption was dominated by rhyodacitic magma with minor amounts of mafic dacite (4%) and andesite (1%). Mandeville *et al.* (1996) proposed that the magma

chamber was compositionally and thermally zoned with rhyodacite at ~880–890°C, more mafic dacite at 890–913°C and andesite at 980–1000°C. At the onset of increasing seismic activity prior to the 1883 eruption, a thin layer (60 cm) of olive–grey and bluish grey silty ash was deposited on top of the first 30 cm of lighter-coloured dacitic pumice. This grey ash is basaltic in composition and is proposed to be the product of a small volume of basaltic magma ejected in an early phase of the eruption, following the initial ejection of dacitic magma (Francis & Self, 1983). This injection of hot basaltic magma could have been the trigger for the catastrophic rhyodacitic eruption and may be the source of the disequilibrium phenocrysts of anorthite-rich plagioclase in the rhyodacites. This event may also indicate the persistence of basaltic andesite activity, which has continued at Anak Krakatau since 1883.

Whole-rock Sr isotope ratios indicate that fractional crystallization dominates the magmatic processes at Krakatau; the apparently minor role of crustal assimilation is evaluated quantitatively in the next section.

The $\delta^{18}O$ values for the Anak Krakatau lavas and 1883 rhyodacites (Fig. 7b) follow a typical magmatic trend of an ~0·2‰ increase per 5% increase in SiO_2 wt % and are ~0·5‰ higher than the normal $\delta^{18}O$ array of projected values modelled from closed-system crystal–liquid fractionation of a mafic mantle-derived melt (5·7 ± 0·3‰, Eiler *et al.*, 2000; Eiler, 2001; grey field indicating 'normal' array in Fig. 7b, after Bindeman *et al.*, 2004). Although elevated whole-rock $\delta^{18}O$ values of volcanic rocks can be due to modification by post-eruptive processes, such as low-temperature hydration of glassy groundmass or hydrothermal alteration, non-glassy Anak Krakatau basaltic andesites are elevated by the same proportion as glassy 1883 rhyodacites and therefore probably reflect assimilation of a high $\delta^{18}O$ contaminant by both the modern and the 1883 magmas.

For oxygen, binary mass-balance calculations indicate that mafic mantle-derived melts may have undergone between 3 and 30% contamination before eruption at Krakatau. Estimates depend on the assimilant composition and recognition that the isotope oxygen measurements may not represent their original value owing to hydrothermal alteration of the xenoliths or decarbonation of carbonates. In fact, the metasedimentary cordierite-bearing xenolith population exhibits a wide range in $\delta^{18}O$ and some xenoliths have seemingly exchanged oxygen with the host magma during high-T metamorphism (see Feeley & Sharp, 1995; Hansteen & Troll, 2003; Aparicio *et al.*, 2006). The xenolith $\delta^{18}O$ values (3·2–13·6‰) extend both below and above values typical for mantle-derived melts, indicating a variety of interaction processes of the sedimentary xenoliths with Anak magmas, with an increasing component of a high-temperature fluid overprint for the low $\delta^{18}O$ xenoliths (e.g. Hansteen & Troll, 2003).

Quantitative modelling

Least-squares mass-balance modelling (major elements)

The evolution of the contemporary Anak Krakatau-type magma to the 1883 rhyodacite composition was modelled by least-squares mass-balance modelling using bulk-rock and analysed mineral compositions. Pumice sample K.S.P-03 (1883 rhyodacite) can be derived from a parental magma of basaltic andesite composition (e.g. K.L-01) (see Table 8 for the mass-balance calculations). The model reproduces well ($\Sigma r^2 = 0{\cdot}083$) the composition of the 1883 obsidian from the Anak magma composition of 55·5 wt % SiO_2, with 45·5% crystallization of an assemblage of plagioclase, clinopyroxene, orthopyroxene and magnetite. The results correspond closely to the actual phenocryst abundances and their relative proportions recorded in our point counting analyses, and are also similar to models calculated by Mandeville *et al.* (1996) using a pre-1883 andesite as a parent for the 1883 eruption. However, the phase percentage of ~13% derived for orthopyroxene contrasts with a value of only ~2% for the true phenocryst population (see Table 3).

Rayleigh fractional crystallization modelling (REE and trace elements)

Rayleigh crystallization modelling of REE and incompatible trace elements using appropriate mid-range partition coefficients for basalt–andesite–dacite compositions from the GERM database (http://earthref.org/GERM/index.html and Electronic Appendix 2) are shown in Fig. 10a and b. The models simulate 25%, 35% and 45% crystallization (with remaining liquid, $f = 0{\cdot}75$, 0·65 and 0·55) of the assemblage plagioclase, clinopyroxene, orthopyroxene and magnetite, using phase proportions calculated from the least-squares modelling (Table 8).

Calculated chondrite-normalized REE patterns (Fig. 10a) show a close match at $f = 0{\cdot}55$, whereas the primitive-mantle normalized multi-element patterns for the 1883 Krakatau rocks (Fig. 10b) show small but notable deviations relative to the model abundances (see Table 5). The multi-element patterns show enrichment of Cs, Rb, Ba, K and Pb (LILE) and Th, U, Nb and Zr (HFSE) relative to the modelling results, but relative depletions in Sr, P and Ti. Depletions in Sr, P and Ti in the 1883 pumices and obsidians can be attributed to crystallization of feldspar, apatite and iron–titanium oxides, respectively.

These models also indicate that although the 2002 and 1883 magmas have evolved from similar parent magmas and that fractional crystallization of Anak Krakatau-type basaltic–andesite magma can create rhyodacitic melt similar to the 1883 eruption, secondary processes may also be in effect. In particular, Rayleigh fractional crystallization modelling predicts lower abundances of LILE (including Pb) than determined in the 1883 rhyodacites, which may be explained by AFC-style processes. Magmas

Table 8: Least-squares calculations modelling crystallization from an initial magma composition of an Anak Krakatau basaltic andesite to produce an 1883 rhyodacite

Component	Initial	Final	Phase compositions (normalized to 100%)				
	magma K.L-01	magma K.S.P-03	Opx	Cpx	Ca-plag	Magnetite	
SiO_2	54·92	63·06	51·99	48·57	45·86	0·00	
TiO_2	1·11	1·00	0·37	1·97	0·01	25·41	
Al_2O_3	18·13	16·14	1·34	5·93	33·74	1·78	
FeO_t	8·50	5·43	23·79	8·83	0·68	70·22	
MgO	4·34	2·07	20·73	13·76	0·05	2·59	
CaO	8·56	5·10	1·78	20·26	18·40	0·00	
Na_2O	3·53	5·54	0·00	0·67	1·24	0·00	
K_2O	0·91	1·66	0·00	0·00	0·02	0·00	
P_2O_5	0·00	0·00	0·00	0·00	0·00	0·00	
Total	100·00	100·00	100·00	99·99	100·00	100·00	
		$\sum(R^2)$	Phase % (relative to initial magma)				Total
							crystallized
		0·083	−13·36	−2·99	−26·51	−2·62	−45·48

contaminated by silicic crustal partial melts tend to produce patterns with elevated levels of Cs, Rb, Ba, Th and Pb relative to pure fractional crystallization products (e.g. DePaolo, 1981; Troll *et al.*, 2005; Meyer *et al.*, 2009, and references therein).

Modelling assimilation with fractional crystallization—AFC and EC-AFC models (trace elements and isotopes)

To constrain our models further, we used the energy-constrained assimilation and fractional crystallization model (EC-AFC) of Spera & Bohrson (2001) and also a classical AFC model (DePaolo, 1981) to investigate the influence of contamination by a variety of potential crustal assimilants. Three possible assimilants from the Krakatau system were considered: AK.Xla-05 x (a gabbroic xenolith from the Anak Krakatau lavas); K.S.SC-05/06 (a carbonate sedimentary clast from within the 1883 deposits); K.S.SC-07 (a quartzo-feldspathic siltstone clast from within the 1883 deposits); plus a fourth hypothetical granite composition to approximate the Cretaceous quartz monzonite basement [from Williams *et al.* (2009), selected because of the full reported dataset for a quartz monzonite sample]. As the host of the phenocrysts investigated by LA-ICP-MS and a representative Anak Krakatau basaltic andesite, sample AK1 was chosen to represent the parental magma for all models (Figs. 11 and 12), and bulk distribution coefficients (D_0 values) for the modelled elements were calculated using appropriate mid-range partition coefficients from the GERM database (Electronic Appendix 2). Ratios of assimilation to fractional crystallization (r), varying from 0·1 to 0·5, were investigated using simple AFC models. For comparative purposes, Fig. 11a and b demonstrates each contaminant with an r of 0·3. The AFC models produced similar mixing trajectories to those of the EC-AFC simulations and therefore only the energy-constrained models will be discussed below.

We have modelled magma compositional trajectories with progressive cooling and concomitant contamination of the Anak Krakatau magmas according to the model parameters in Table 9. Initial melt temperatures of 1200°C ($T_{\mathrm{lm}} = T_{\mathrm{m}}^{\circ}$) were selected, and cooled to an equilibration temperature of 890°C (T_{eq}) constrained by Fe–Ti oxide temperatures for the 1883 rhyodacite (Mandeville *et al.*, 1996). We then modelled intrusion into crust with ambient temperatures of 300, 500, 700 and 900°C (T_{a}°), and in Fig. 11c and d we plot trajectories for an initial crustal temperature of 500°C.

We investigated a range of solidus temperatures (T_{s}) from 700 to 850°C and liquidus temperatures (T_{la}) from 800 to 1000°C; these did not produce significantly large differences at the amount of melting considered. For Fig. 11, T_{s} and T_{la} were assumed to be 750°C and 850°C respectively and a local geothermal gradient was taken to be ~70°C km^{-1} (as determined in well C-1SX). Bulk D values for Sr, Nd and Th in the carbonate clast

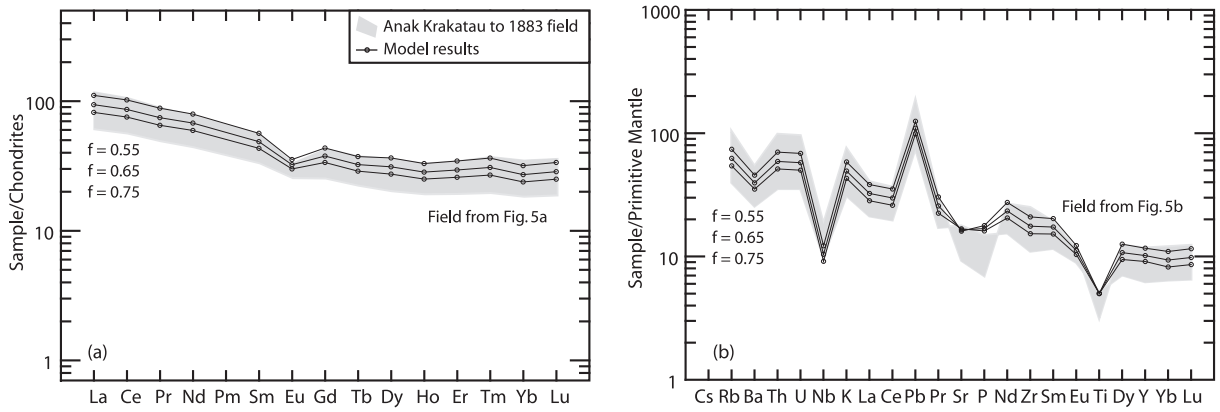

Fig. 10. Fractional crystallization models for 25%, 35% and 45% crystallization (fraction of remaining liquid, $f = 0{\cdot}75$; 0·65 and 0·55) shown as (a) chondrite-normalized REE patterns and (b) primitive mantle-normalized multi-element patterns (shaded area is the field bounded by Anak Krakatau basaltic andesites and 1883 rhyodacites as shown in Fig. 5a and b).

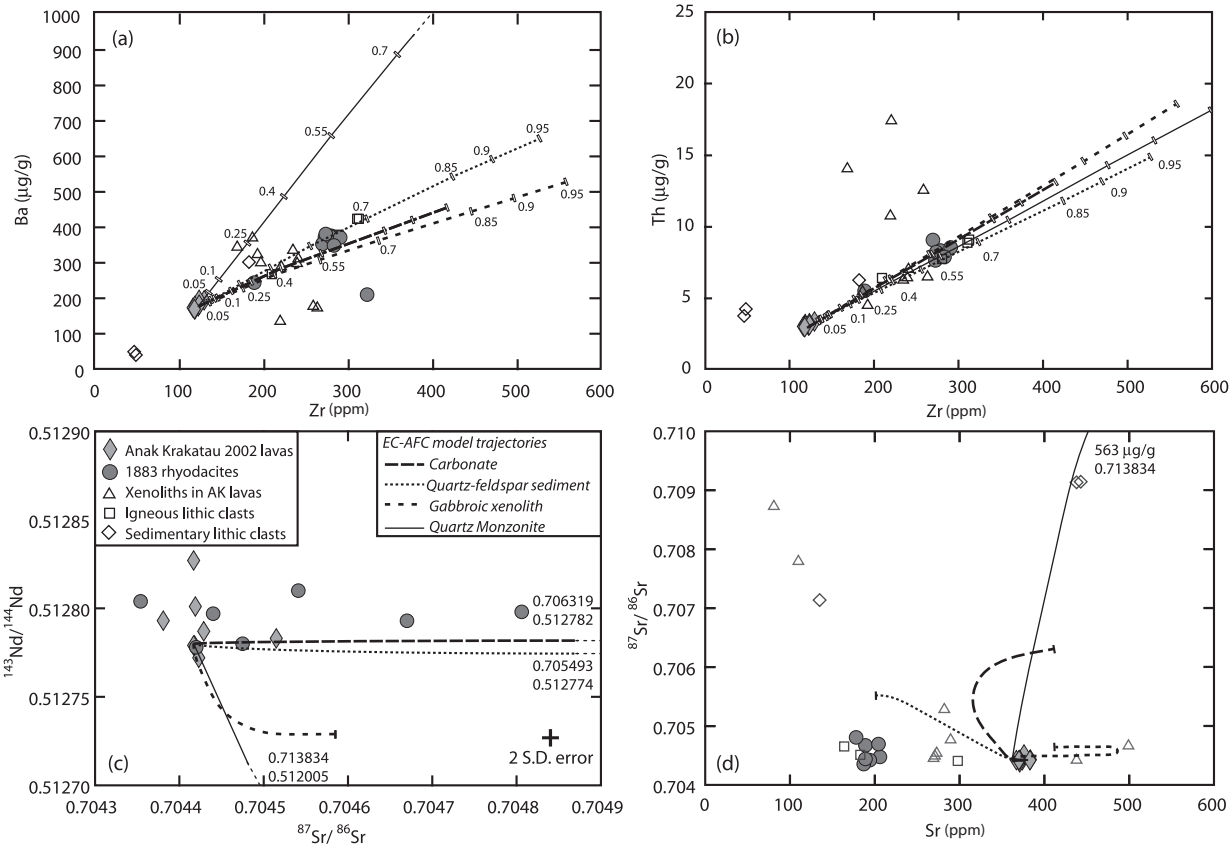

Fig. 11. Simple assimilation and fractional crystallization (AFC) models showing (a) Ba vs Zr and (b) Th vs Zr (in ppm) for increments of f (where f is fraction of remaining liquid). The model results plotted are representative of all trace elements investigated. Four possible contaminants are modelled, a carbonate (long-dash line, sample K.S.SC-05/06), a quartz–feldspathic sediment (dotted line, sample K.S.SC-07), a gabbroic xenolith (short-dash line, sample AK.Xla-05 x) and a hypothetical quartz monzonite (continuous line). Only results for $r = 0{\cdot}3$ are shown for ease of correlation. Results from energy-constrained assimilation and fractional crystallization simulations (EC-AFC) are shown in (c) for $^{143}Nd/^{144}Nd$ vs $^{87}Sr/^{86}Sr$ and (d) for $^{87}Sr/^{86}Sr$ vs Sr concentration (ppm). Trajectories of projected magma compositions are plotted for each of the four considered assimilants, with dashed lines and equilibrium compositional values marked if the trajectory extends off the diagram.

Table 9: Parameters for EC-AFC modelling

Equilibration parameters					
Initial temperature of magma	T_m^o	1200	°C		
Liquidus of magma	T_{lm}	1200	°C		
Initial temperature of wallrock	T_a^o	500	°C		
Liquidus temperature of assimilant	T_{la}	850	°C		
Solidus temperature	T_s	750	°C		
Specific heat, magma	c_{pm}	1484	J kg^{-1} K^{-1}		
Specific heat, assimilant	c_{pa}	1388	J kg^{-1} K^{-1}		
Heat of crystallization	h_{cry}	396000	J kg^{-1}		
Heat of fusion	h_{fus}	250000	J kg^{-1}		
Compositional parameters	Sr	Nd	Th	Pb	U
AK1 primary magma (bulk D0 calculated from GERM Kd values)					
Concentration	383	21	3·034	4·492	0·739
Bulk D0	1·136	0·087	0·014	0·264	0·013
Isotope	87Sr/86Sr	143Nd/144Nd			
Ratio	0·704417	0·512779			
AK·Xla-05x, short-dashed trajectory, gabbroic xenolith					
Concentration	499·2	22·687	10·69	3·367	2·457
Bulk D0	0·6	0·06	0·05	0·005	0·005
Isotope	87Sr/86Sr	143Nd/144Nd			
Ratio	0·704659	0·512669			
K·S·SC-05 or -06, long-dashed trajectory, carbonate sediment					
Concentration	443	7·781	4·142	6·718	1·235
Bulk D0	1·8	0·1	0·05	0·005	0·005
Isotope	87Sr/86Sr	143Nd/144Nd			
Ratio	0·70714	0·51279			
K·S·SC-07, dotted trajectory, quartzo-feldspathic siltstone					
Concentration	135	23·252	6·175	10·775	1·515
Bulk D0	0·7	0·1	0·05	0·005	0·005
Isotope	87Sr/86Sr	143Nd/144Nd			
Ratio	0·707133	0·512769			
Quartz monzonite (theoretical), line trajectory					
Concentration	700	40	10	25	2·6
Bulk D0	1	0·06	0·05	0·005	0·005
Isotope	87Sr/86Sr	143Nd/144Nd			
Ratio	0·716482	0·51151			

(K.S.SC-05/06), siltstone clast (K.S.SC-07), gabbroic xenolith (AK.Xla-05x) and quartz monzonite are reported in Table 9.

Modelled trajectories for magma compositions from 1200°C to 890°C plot as curves in Fig. 11c and d with the quartzo-feldspathic siltstone (dotted line), the gabbroic xenolith (short-dashed line), the carbonate sedimentary clast (long-dashed line) and the hypothetical quartz monzonite (continuous line) being shown. The thermal constraints of the models cause the trajectories to trace identical paths initially whilst the surrounding crust heats up, and fractional crystallization dominates the system (horizontal initial path at 0·7044 in Fig. 11d). Owing to the release of latent heat, for each degree of heat lost from the magma body, the crust temperature rises by 3·5°C, from the ambient T of 500°C, until it reaches the solidus (750°C) and anatectic melt starts to become assimilated into the magma body. Once partial melting occurs, the rate of temperature rise in the country rock decreases with the rise in enthalpy requirements of anatexis

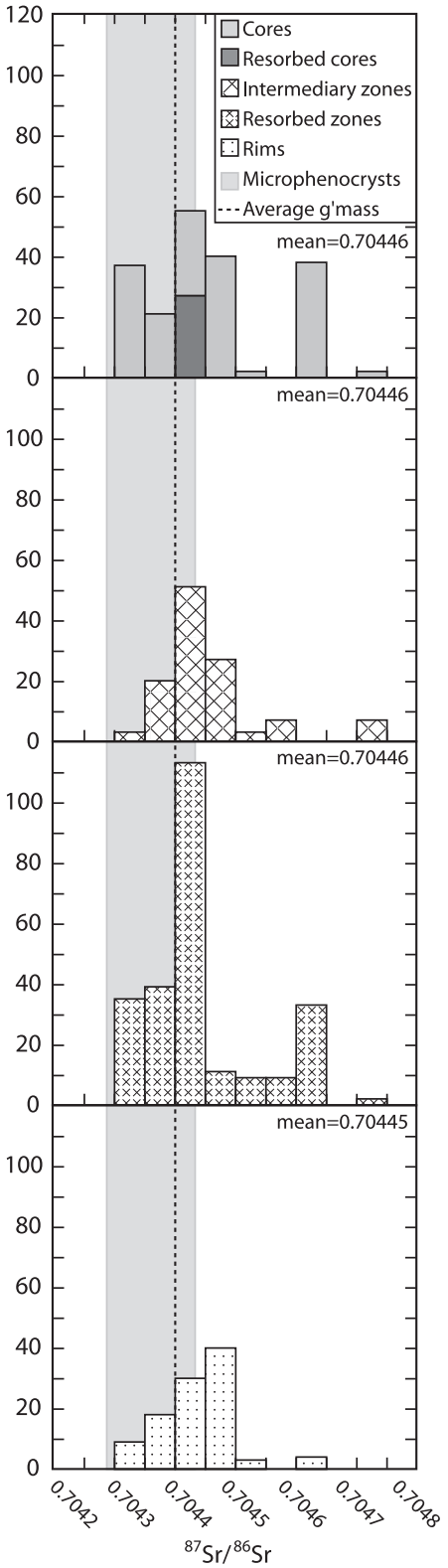

Fig. 12. Histograms of $^{87}Sr/^{86}Sr$ showing compositional variation amongst 13 plagioclase phenocrysts in a single thin section (sample AK1). Cores, rims and intermediary zones were identified from BSE images and analysed for $^{87}Sr/^{86}Sr$ by LA-ICP-MS. By correlating overlapping laser troughs and EMP spot values, binned compositions are plotted on separate histograms to provide a mainly qualitative comparison of core, intermediary zone and rim Sr isotope ratios. The bimodality for plagioclase core and intermediary zone values and the contrasting unimodal distribution of slightly elevated $^{87}Sr/^{86}Sr$ values from crystal rims should be noted. The dashed line marks the average microphenocryst value and the grey bar demonstrates the range for all microphenocrysts including analytical uncertainties (representative of the $^{87}Sr/^{86}Sr$ of the host magma).

(Bohrson & Spera, 2001). However, xenolith entrainment and disaggregation through partial melting along grain boundaries, as opposed to bulk melting alone, can reduce the energy demands for assimilation to a certain degree (e.g. Beard *et al.*, 2005), and may be anticipated as a relevant process in the context of the complex crystal cargo of Anak Krakatau eruptive products (see below).

Variation in $^{87}Sr/^{86}Sr$ plotted against $^{143}Nd/^{144}Nd$ (Fig. 11c) suggests that either the carbonate or quartzo-feldspathic sedimentary clasts may be potential contaminants; for $^{87}Sr/^{86}Sr$ plotted against Sr concentration in the melt (Fig. 11d), the quartzo-feldspathic siltstone provides a closer match. The traditional AFC models in Fig. 11a and b corroborate this, with Ba plotted against Zr and Th against Zr, and also with other trace elements not shown here. Employing these parameters, the 1883 rhyodacite can be produced by 45–50% crystallization of an Anak Krakatau-type basaltic andesite magma with contamination by quartzo-feldspathic sediment from the crust that underlies Krakatau volcano with a ratio of assimilation to crystallization (r) of 0·1–0·3. After 45% crystallization with $r = 0{\cdot}1$, assimilation would be 5%, whereas with $r = 0{\cdot}3$, assimilation would equate to 13%. Similar r values of 0·05–0·3 are required to replicate the observed 0·6‰ enrichment in $\delta^{18}O$ of the Krakatau magmas relative to oxygen isotope values expected for primitive mantle-derived melts.

These results are comparable with our EC-AFC models where $r < 0{\cdot}2$ will produce Sr isotopic ratios of 0·7044–0·7046, and $r = 0{\cdot}2$–$0{\cdot}4$ creates $^{87}Sr/^{86}Sr$ of 0·7046–0·7047. Therefore, r values from zero to 0·4 can produce the Sr isotopic ratios most commonly found within the 2002 Anak plagioclase phenocryst zones. The very highest $^{87}Sr/^{86}Sr$ ratios in the outermost rim of plagioclase AK1-pl03 (0·7048, Fig. 8b) would require 45% crystallization and 23% assimilation of anatectic melt, with an r of 0·5. Sr isotopic ratios of ~0·7048 are typical of the 1883 rhyodacites (Fig. 13), indicating that plagioclase AK1-pl03 may be an 1883 antecryst. We therefore conclude that shallow contamination and assimilation is an important late-stage process influencing the evolution of the Krakatau lavas.

Plagioclase phenocryst laser ablation analyses

Major element compositions of plagioclase are controlled by temperature, pressure, melt composition and water content,

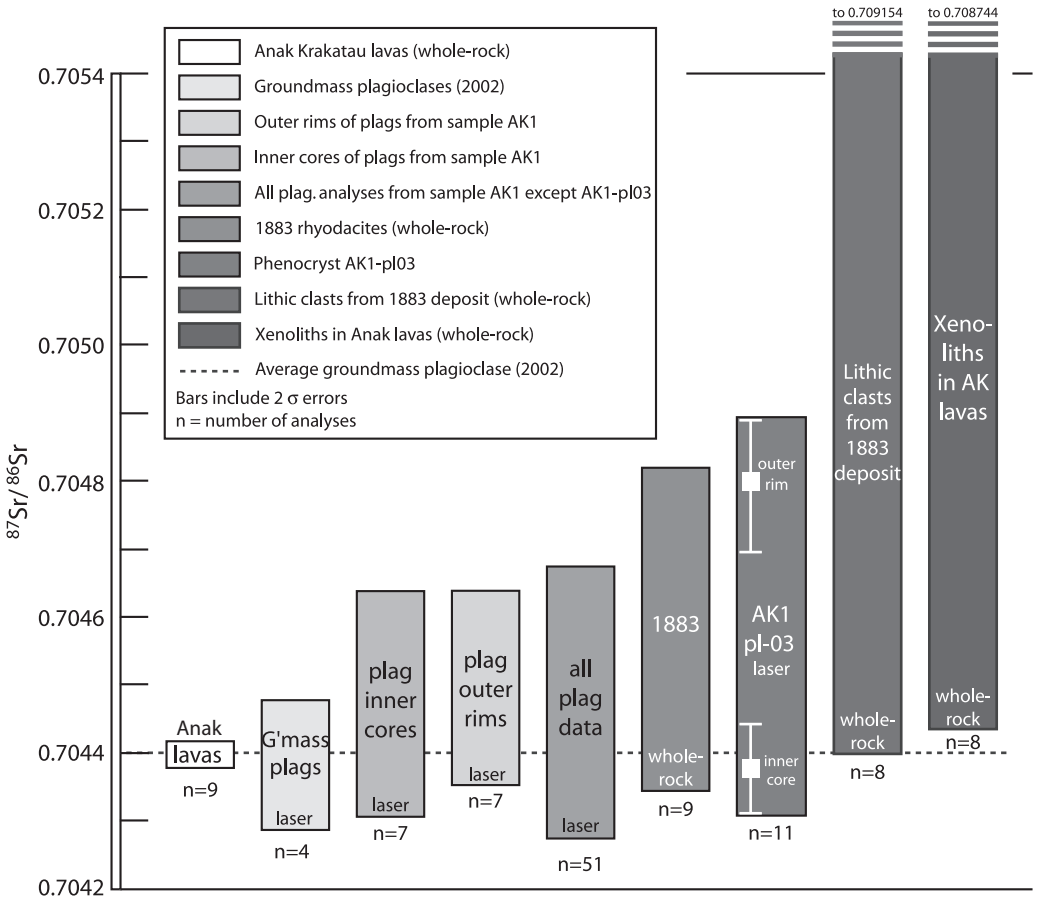

Fig. 13. Bar chart displaying the $^{87}Sr/^{86}Sr$ variation for all the geochemical groups at Krakatau. Whole-rock samples (labelled) were analysed by TIMS or MC-ICP-MS and plagioclase cores, rims and groundmass microphenocrysts by LA-ICP-MS. (Note the increased range of $^{87}Sr/^{86}Sr$ in the 1883 deposits relative to the Anak lavas, reflecting a strong crustal involvement in the petrogenesis of the 1883 rhyodacites.)

which are all subject to variation even within a chemically closed system. In contrast to this, radiogenic isotope compositions will vary only if the system is open to mass exchange. At constant pressure and H_2O content, the anorthite content of crystallizing plagioclase decreases with increasing fractional crystallization of the melt and related decreasing temperature. Decompression events with changing H_2O pressure (e.g. Blundy *et al.*, 2006), or convection within the magma chamber (Couch *et al.*, 2001), will cause modulations in the An content of plagioclase and can explain features such as that in crystal AK1-pl09 (Fig. 8d), with constant $^{87}Sr/^{86}Sr$ ratios and small spikes in FeO_t content across major An variations ($An_{\Delta 30}$). Low $^{87}Sr/^{86}Sr$ values across the phenocryst indicate that following resorption of an older, recycled crystal core, crystallization of the plagioclase intermediary zone and outer rim occurred in a relatively less contaminated melt, similar in composition to the groundmass plagioclase phenocrysts.

However, for some of the analysed plagioclase crystals from Anak Krakatau, an increase in $^{87}Sr/^{86}Sr$ towards the rims is identified, indicating progressive crustal contamination of the magma during late crystal growth (e.g. AK1-pl01 and AK1-pl03, Fig. 8a and b). Cores with high anorthite content are coupled with lower $^{87}Sr/^{86}Sr$, and a decrease in anorthite towards the outer zones occurs with a general increase in $^{87}Sr/^{86}Sr$. These crystals can be grouped together as they are broadly consistent with an AFC-style process (i.e. increased radiogenic input with increased degree of differentiation). Phenocryst AK1-pl04 (Fig. 8c) also displays complex variations in its Sr isotope composition, indicating crystallization from a melt with variable $^{87}Sr/^{86}Sr$.

A second group of crystals showing greater degrees of resorption also exist within the Anak Krakatau 2002 basaltic andesites (Fig. 9a and b). Electron microprobe profiles reveal large variations in An content and non-systematic changes in $^{87}Sr/^{86}Sr$ across these sieve-textured plagioclase phenocrysts. This complex zonation, to the extent that no correlations remain between anorthite and $^{87}Sr/^{86}Sr$, is consistent with a complex interplay of episodes of prolonged growth and resorption events during open-system magmatic processes.

Variations in $^{87}Sr/^{86}Sr$ within the plagioclase populations are summarized in the histograms shown in Fig. 12. By aligning laser trough positions against the EMP profiles, a quantitative analysis of core, intermediary zone and rim plagioclase $^{87}Sr/^{86}Sr$ (measured by LA-ICP-MS) is shown. This displays a clear bimodality between ratios of ~0·7044 and ~0·7046 for plagioclase cores and intermediary zones and a unimodal distribution of outer rim compositions of ~0·7045. The Sr isotope composition of the final 2002 Anak Krakatau melt can be approximated by the groundmass plagioclase and phenocryst rims at ~0·7044 (dashed line in Fig. 12 indicates the average microphenocryst value). The higher $^{87}Sr/^{86}Sr$ of the crystalline assemblage must be inherited from the country rock or recycled from previously contaminated magma chamber products through which the melts passed en route to the surface (e.g. crystal AK1-pl03, Fig. 8b).

A small proportion (~0·5%) of plagioclase crystals with very high An contents (>90% An) was detected in lavas erupted from 1927 to 2002 (Fig. 3b), and these are proposed to be antecrysts and/or xenocrysts from earlier cumulates and magma batches at depth (Camus *et al.*, 1987; Mandeville *et al.*, 1996; this study). These recycled crystals now form cores, with late overgrowth of higher $^{87}Sr/^{86}Sr$ rims forming in shallow magma chambers and during ascent.

In Fig. 13, $^{87}Sr/^{86}Sr$ laser analyses of cores and rims of plagioclase phenocrysts and groundmass plagioclase microcrystals from Anak Krakatau are compared with bulk-rock samples of contemporary Anak Krakatau lavas, 1883 rhyodacites, siliciclastic and dolomitic–carbonate clasts from the local crust, and metasedimentary and plutonic xenoliths. Whole-rock analyses of nine Anak Krakatau lavas show the narrowest variation in $^{87}Sr/^{86}Sr$ ($0{\cdot}70440 \pm 5$), which contrasts strongly with the wide variation in values of the pumices and obsidians from the 1883 rhyodacite eruption. The Anak Krakatau lavas contain a wide variety of phenocrysts, represented in Fig. 13 as 'all plag data'. The zoned plagioclase phenocrysts are commonly more radiogenic than the groundmass microcrystals (dashed line indicates the average microcrystal value). Also, crystal AK1-pl03, the outer rim of which has $^{87}Sr/^{86}Sr$ of $0{\cdot}7048 \pm 1$, is considerably more radiogenic than any other plagioclase from Anak Krakatau. This high $^{87}Sr/^{86}Sr$ value provides direct evidence for the inclusion of crystals from more contaminated melts and/or crystals from a crustal source (e.g. Beard *et al.*, 2005).

Zoning of major and trace elements may occur in response to decompression pulses or chemical changes (e.g. Davidson & Tepley, 1997; Blundy *et al.*, 2006; Ginibre & Wörner, 2007), however, these zones would not be accompanied by changes in Sr isotope composition. These large, beyond analytical error, variations in $^{87}Sr/^{86}Sr$ between discrete zones in plagioclase crystals are evidence that they grew in a magma that had its composition changed by assimilation of melt and xenocrysts and/or antecrysts within the Anak Krakatau magmatic system.

IMPLICATIONS FOR ANAK KRAKATAU

Differentiation in the form of fractional crystallization leaves a robust major element signature and takes place primarily in the crust, at pressures and temperatures over which observed and geochemically inferred phases are stable (e.g. plagioclase, olivine, pyroxene and oxides). However, the isotopic compostion of Sr should remain unchanged by geochemically 'closed-system' fractionation processes. On a crystal scale, we identified variations in $^{87}Sr/^{86}Sr$ in plagioclase, which are compositionally attributable to assimilation of sediment at shallow crustal levels within the volcano's plumbing system.

Clinopyroxene $^{3}He/^{4}He$ values of $6{\cdot}9 \pm 1{\cdot}8$ and Mg# of ~75 (Gasparon *et al.*, 1994) and fumarole gas values of $(5{\cdot}2–7{\cdot}2) \pm 0{\cdot}12$ (Blythe *et al.*, 2009) signify low-pressure differentiation processes at Anak Krakatau with assimilation of crustal materials clearly indicated. Xenolith digestion within magmatic systems has been shown to occur sufficiently rapidly (days to weeks at most) and may remove nearly all physical evidence of wall-rock assimilation well within the typical repose periods of arc volcanoes (Dungan, 2005). Assuming xenolith disintegration to be accomplished by processes akin to, for example, reactive bulk mixing (Beard *et al.*, 2005; see Fig. 2), a fully disaggregated xenolith will not only have contributed partial melt, but will also have released its remaining crystals, thus contributing to the complex crystal cargo in the Anak lavas. Given that the sedimentary pile beneath Anak is probably some 5 km thick, and that magma storage demonstrably occurs within this shallow level (Dahren *et al.*, 2012), it is conceivable that sedimentary xenoliths that completely disintegrated into the magmatic system have provided nuclei for further crystal growth in the shallowest Anak system (i.e. ≤2–3 km). Considering the common occurrence of pyro-metamorphic minerals within the abundant siliciclastic and pumiceous xenoliths and the large cordierite xenocrysts in Anak lavas, it is likely that many of the metasedimentary xenoliths record assimilation of pre-heated wall-rock (i.e. from a contact aureole). This implies that uptake of crustal melts may have been continuing and steady state, despite xenoliths having been incorporated into the magma only shortly before eruption.

The petrology and phenocryst Sr isotope record from Krakatau suggest multi-stage magmatic evolution in a shallow system. This is consistent with geophysical observations (Harjono *et al.*, 1989; Jaxybulatov *et al.*, 2011) that predict irregular pockets of magma in the upper low-velocity zone (~7 km). A plexus of smaller magma chambers or pockets in the shallowest crust is beyond the resolution of these

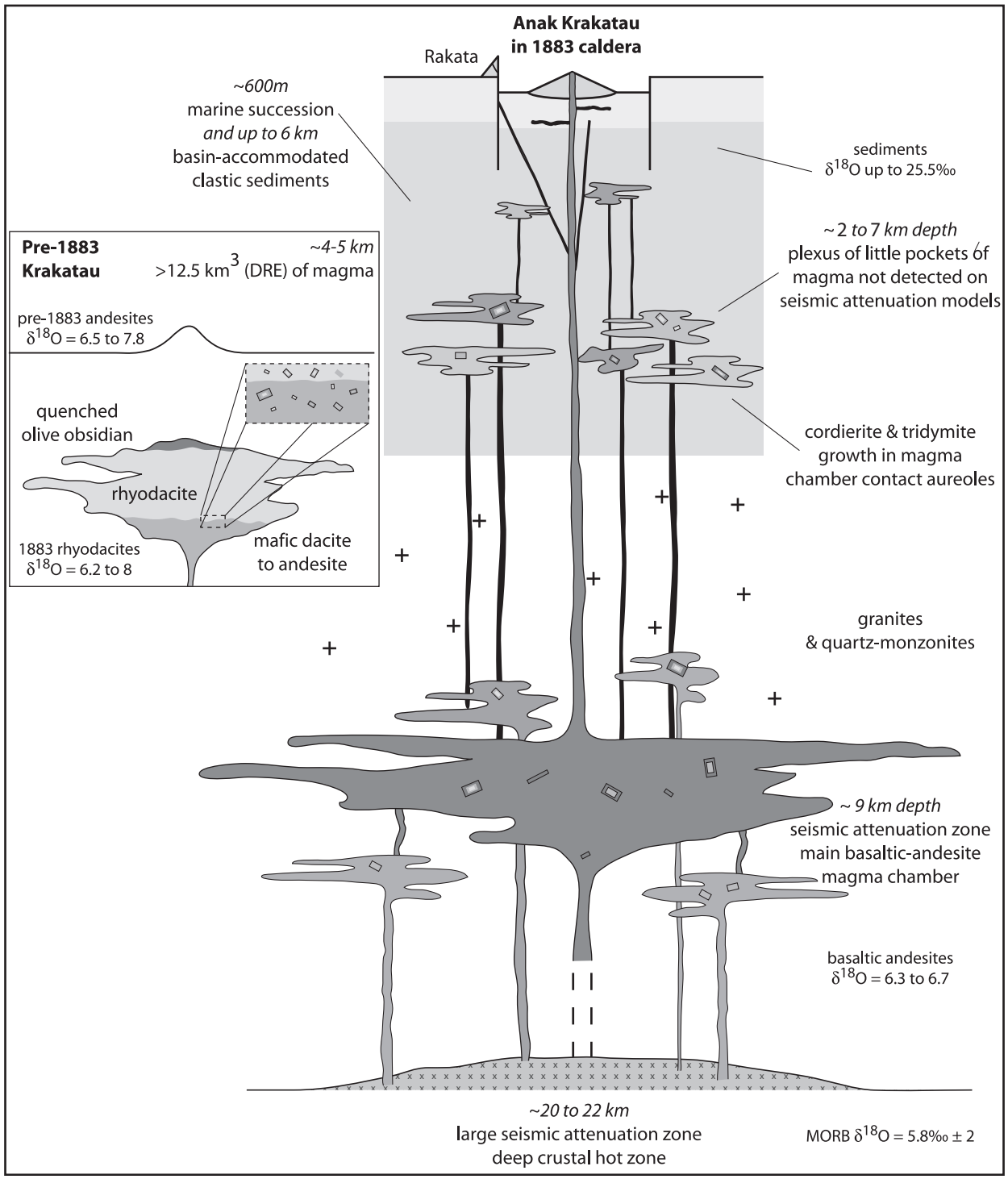

Fig. 14. Schematic illustration of the magma plumbing system for the Krakatau volcanic complex (not to scale). The 1883 rhyodacites are genetically related to the Anak Krakatau basaltic andesite magma in the sense that both derive from a similar parent magma. On a crystal scale we identified variations in $^{87}Sr/^{86}Sr$ in plagioclase in the Anak lavas, which are compositionally attributable to assimilation of sediment at shallow crustal levels ($\leq$6 km) within the volcano's uppermost plumbing system. Partially digested xenoliths containing pyro-metamorphic minerals cordierite and tridymite underline that incorporation of crustal materials occurred high in the crust ($\leq$2 kbar). Geophysical evidence refutes the existence of a large-volume shallow magma chamber beneath Anak Krakatau at present and current Anak Krakatau activity is probably sourced from a plexus of small and partly crystalline, semi-independently evolving pockets of magma that are not always clearly detectable by geophysical means (e.g. Jaxybulatov *et al.*, 2011).

surveys, but is clearly supported by evidence of sediment contamination and the presence of contact metamorphic metasedimentary xenoliths. This could be a major cause for the lack of uniform populations of phenocrysts and the 2002 Anak Krakatau products could be a mix of two or more magma pockets fed through a common conduit (Fig. 14).

Although the diversity in texture among the studied plagioclase phenocrysts and the wide range in Sr isotope composition may not completely preclude simple processes of magma mixing (Ruprecht *et al.*, 2008), the lack of geophysical evidence for a large, shallow magma chamber leads us to conclude that the Anak Krakatau activity is now sourced from a number of small, semi-independently evolving pockets of magma through which the magmas experience variable ascent and storage conditions in the shallow crust. For example, the distinctive evolved andesite eruption in 1981 (Camus *et al.*, 1987) may have been sourced from a small volume, relatively evolved magma pocket prior to the continuation of basaltic andesite activity [see Gamble *et al.* (1999) and Nakagawa *et al.* (1999); and Price *et al.* (2005) for Ruapehu Volcano, New Zealand]. Groundmass plagioclase crystals with lower $^{87}Sr/^{86}Sr$ than the outer rims of larger phenocrysts may indicate that crystals from these small-volume chambers situated within the shallow crust may be subsequently recycled into more primitive magmas en route to the eruption site or reflect mixing of contrasting magma batches.

In an area subject to frequent faulting such as the Sunda Strait, magma plumbing systems and tectonic parameters controlling mixing may change swiftly from one eruption to the next (even within a single eruption sequence) leading to apparently random short-term trends. The location of the Krakatau volcanic complex at the intersection of a graben zone and the active seismic belt, a tectonic situation distinct from that of other Javan and Sumatran volcanic centres, may be related to this wider compositional range (Harjono *et al.*, 1991). Detailed chronological studies are required to identify more systematic trends in the long term, and further study of anorthite and trace element compositional profiles in plagioclase may lead to an estimation of the timescales involved in assimilation of magmas at Anak Krakatau (see Costa *et al.*, 2003; Chadwick *et al.*, 2007; Ruprecht & Wörner, 2007).

A similar sequence of episodically valved eruptions from a shallow chamber system, with a potentially continuous magma supply from a deeper crustal reservoir, has been successfully modelled from geodetic and eruption records at Soufrière Hills volcano on Montserrat (Elsworth *et al.*, 2008) and Shiveluch, Kamchatka (Humphreys *et al.*, 2006). A lack of textural overlap between phenocryst types at these locations suggests that populations were spatially or temporally isolated during crystallization, with sieve-textured plagioclase resulting from mixing of a more felsic magma with the host andesite.

The present-day Anak Krakatau activity may represent the initial stages of an evolutionary cycle that could culminate in the type of catastrophic rhyolite eruption witnessed in 1883 and which produced the even larger pre-1883 caldera. Alternatively, it may represent the culmination of a cycle of activity, as mafic magma that triggered the 1883 event by remobilization finally reaches the surface. Cyclic activity at Krakatau was first proposed by van Bemmelen (1949) and discussed further by Camus *et al.* (1987). The latter suggested that the system had evolved to evolved-andesite or even dacite by 1981. The return to basaltic andesite compositions since the 1981 evolved andesite indicates that considerably more time is required to prime Krakatau for another caldera-forming rhyodacite eruption (10^3–10^4 years; see Jicha *et al.*, 2005).

Geochemical analyses of samples from other localities in the Sunda Strait area (Ujung Kulon and Kotaagung; Nishimura *et al.*, 1986) in addition to those from Krakatau (Oba *et al.*, 1982, 1992) have been used to suggest that ignimbrites may be sourced from re-melting of lower crustal materials. Our data indicate that the 1883 rhyodacite is genetically related to the Anak Krakatau basaltic andesite magma via shallow crustal AFC-style processes and xenocryst incorporation with crustal recycling clearly influencing its evolution from mafic to felsic compositions.

CONCLUSIONS

Our analysis of major and trace element data combined with whole-rock $\delta^{18}O$, Sr, and Nd isotope data for the Krakatau volcanic complex, in addition to *in situ* chemical data (EMP and laser ablation Sr isotope ratios) for plagioclase from the most recent eruptive rocks, reveals a picture of a complex plumbing system of many small but shallow magma chambers or pockets beneath the present Anak Krakatau edifice. A repetition of caldera-forming eruptions at the Krakatau Complex in the past suggests the presence of a continuing and long-lived system with potential periodicities of 10^3 or 10^4 years, with present eruptions of basaltic andesite being part of the crust conditioning process associated with eventual accumulation of a new rhyodacite magma body.

Crustal contamination is a continuing process throughout the crust below Krakatau as evidenced by large $^{87}Sr/^{86}Sr$ variations within plagioclase phenocrysts and the abundance of silicic metasedimentary xenoliths assimilated partly at high levels in the crust. To predict the 1883 magma composition (whole-rock and AK1-pl03 antecryst), both traditional AFC and EC-AFC models require 45% crystallization of an Anak Krakatau-type magma, with up to 23% assimilation of anatectic melt from a local quartzo-feldspathic basement sediment. To reproduce the variation seen in the 2002 Anak Krakatau whole-rock analyses and plagioclase phenocrysts, 5–13% assimilation is required. Modelling of whole-rock data therefore has low

sensitivity to the complex *in situ* variations revealed by the crystal isotope stratigraphy. The main crystal assemblages seen in the Anak Krakatau lavas are hence controlled by fractional crystallization, xenolith disintegration and currently relatively low levels of anatectic melt input. The latter two processes, however, are likely to increase in relevance with increasing differentiation of erupted melts, such as the rhyodacites erupted in 1883.

ACKNOWLEDGEMENTS

Assistance in the field from Lothar Schwarzkopf, Oli Spieler and Mas Mahjum is greatly appreciated. In addition, we are grateful to Nic Odling at Edinburgh University, Neil Kearney at Trinity College, Dublin, Fayrooza Rawoot at University of Cape Town, Andy Tindle at the Open University, and Anne Kelly, Vinnie Gallagher and Valerie Olive at the Scottish Universities Environmental Research Centre (SUERC) for technical assistance in the laboratory. We thank Jane Chadwick, Sebastian Wiesmaier, Börje Dahren, Bruce Charlier, Godfrey Fitton, Michael Krumbholz and Malte Junge for their helpful comments and contributions, and we would like to thank Brian Jicha, Kurt Knesel, Philipp Ruprecht and Gerhard Wörner for their thorough and helpful comments, which have substantially improved this paper.

FUNDING

This project was funded by a Science Foundation Ireland grant (04/BR/ES0011) to J.G. and V.R.T., and a Swedish Science Foundation grant to V.R.T.

SUPPLEMENTARY DATA

Supplementary data for this paper are available at *Journal of Petrology* online.

REFERENCES

Abratis, M., Schminke, H.-U. & Hansteen, T. H. (2002). Composition and evolution of submarine volcanic rocks from the central and western Canary Islands. *International Journal of Earth Sciences* **91**, 562–582.

Annen, C., Blundy, J. D. & Sparks, R. S. J. (2006). The genesis of intermediate and silicic magmas in deep crustal hot zones. *Journal of Petrology* **47**, 505–539.

Aparicio, A., Bustillo, M. A., Garcia, R. & Araña, V. (2006). Metasedimentary xenoliths in the lavas of the Timanfaya eruption (1730–1736, Lanzarote, Canary Islands): metamorphism and contamination processes. *Geological Magazine* **143**, 181–193.

Bachman, O. & Bergantz, G. W. (2004). On the origin of crystal-poor rhyolites: extracted from batholitic crystal mushes. *Journal of Petrology* **45**, 1565–1582.

Bachman, O. & Bergantz, G. W. (2008). Rhyolites and their Source Mushes across Tectonic Settings. *Journal of Petrology* **49**, 2277–2285.

Baschek, G. & Johannes, W. (1995). The estimation of NaSi–CaAl interdiffusion rates in peristerite by homogenization experiments. *European Journal of Mineralogy* **7**, 295–307.

Beard, J. S., Ragland, P. C. & Crawford, M. L. (2005). Reactive bulk assimilation: A model for crust–mantle mixing in silicic magmas. *Geology* **33**, 681–684.

Beauregard, J. L. (2001). Explosive rhyodacitic volcanism: the evolution and frequency of pre-1883 eruptions at Krakatau Volcano, Indonesia, PhD thesis, University of Rhode Island, Providence.

Bindeman, I. N., Ponomareva, V. V., Bailey, J. C. & Valley, J. W. (2004). Volcanic arc of Kamchatka: a province with high-$\delta^{18}O$ magma sources and large scale $^{18}O/^{16}O$ depletion of the upper crust. *Geochimica et Cosmochimica Acta* **68**, 841–865.

Blundy, J. D. & Shimizu, N. (1991). Trace element evidence for plagioclase recycling in calc-alkaline magmas. *Earth and Planetary Science Letters* **102**, 178–197.

Blundy, J., Cashman, K. & Humphreys, M. (2006). Magma heating by decompression-driven crystallisation beneath andesite volcanoes. *Nature* **443**, 76–80.

Blythe, L. S., Troll, V. R. & Hilton, D. R. (2009). Identifying upper crustal contamination along the Java segment of the Sunda Arc, Indonesia. *Geochimica et Cosmochimica Acta Supplement* **73**, A131.

Bohrson, W. A. & Spera, F. J. (2001). Energy-constrained open-system magmatic processes II: application of energy-constrained assimilation–fractional crystallization (EC-AFC) model to magmatic systems. *Journal of Petrology* **42**, 1019–1041.

Borthwick, J. & Harmon, R. S. (1982). A note regarding ClF_3 as an alternative to BrF_5 for oxygen isotope analysis. *Geochimica et Cosmochimica Acta* **46**, 1665–1668.

Brophy, J. G. (1991). Composition gaps, critical crystallinity, and fractional crystallization in orogenic (calc-alkaline) magmatic systems. *Contributions to Mineralogy and Petrology* **109**, 173–182.

Browne, B. L., Eichelberger, J. C., Patino, L. C., Vogel, T. A., Uto, K. & Hoshizumi, H. (2006). Magma mingling as indicated by texture and Sr/Ba ratios of plagioclase phenocrysts from Unzen volcano, SW Japan. *Journal of Volcanology and Geothermal Research* **154**, 103–116.

Camus, G., Gourgaud, A. & Vincent, P. M. (1987). Petrologic evolution of Krakatau (Indonesia): implications for a future activity. *Journal of Volcanology and Geothermal Research* **33**, 299–316.

Chadwick, J. P., Troll, V. R., Ginibre, C., Morgan, D., Gertisser, R., Waight, T. E. & Davidson, J. P. (2007). Carbonate assimilation at Merapi Volcano, Java, Indonesia: insights from crystal isotope stratigraphy. *Journal of Petrology* **48**, 1793–1812.

Charlier, B. L. A., Bachmann, O., Davidson, J. P., Dungan, M. A. & Morgan, D. (2007). The upper crustal evolution of a large silicic magma body: evidence from crystal-scale Rb–Sr isotopic heterogeneities in the Fish Canyon magmatic system, Colorado. *Journal of Petrology* **48**, 1875–1894.

Costa, F., Chakraborty, S. & Dohmen, R. (2003). Diffusion coupling between trace and major elements and a model for calculation of magma residence times using plagioclase. *Geochimica et Cosmochimica Acta* **67**, 2189–2200.

Couch, S., Sparks, R. S. J. & Carroll, M. R. (2001). Mineral disequilibrium in lavas explained by convective self-mixing in open magma chambers. *Nature* **411**, 1037–1039.

Dahren, B., Troll, V. R., Andersson, U. B., Chadwick, J. P., Gardner, M. F., Jaxybulatov, K. & Koulakov, I. (2012). Magma plumbing beneath Anak Krakatau volcano, Indonesia: evidence for multiple magma storage regions. *Contributions to Mineralogy and Petrology* **163**, 631–651.

Davidson, J. P. & Tepley, F. J. (1997). Recharge in volcanic systems: evidence from isotope profiles of phenocrysts. *Science* **275**, 826–829.

Davidson, J. P., Tepley, F. J., Palacz, Z. & Meffan-Main, S. (2001). Magma recharge, contamination and residence times revealed by *in-situ* laser ablation isotopic analysis of feldspar in volcanic rocks. *Earth and Planetary Science Letters* **184**, 427–442.

Davidson, J. P., Morgan, D. J., Charlier, B. L. A., Harlou, R. & Hora, J. M. (2007). Microsampling and isotopic analysis of igneous rocks: implications for the study of magmatic systems. *Annual Review of Earth and Planetary Sciences* **35**, 273–311.

Deegan, F. M., Troll, V. R., Freda, C., Misiti, V., Chadwick, J. P., McLeod, C. L. & Davidson, J. P. (2010). Magma–carbonate interaction processes and associated CO2 release at Merapi Volcano, Indonesia: insights from experimental petrology. *Journal of Petrology* **51**, 1027–1051.

Deer, W. A., Howie, R. A. & Zussman, J. (1992). *An Introduction to the Rock-Forming Minerals*, 2nd edn. Harlow: Pearson Education.

De Neve, G. A. & Sukardjono (1985). Preliminary notes on the subsurface geology in the vicinity of the Krakatau islands, Sunda Strait region. In: Sastrapradja, D. & Soemodihardjo, S. (eds) *Symposium on 100 Years Development of Krakatau and its Surroundings*. Jakarta: Indonesian Institute of Science (LIPI), pp. 59–71.

DePaolo, D. J. (1981). Trace element and isotopic effects of combined wallrock assimilation and fractional crystallization. *Earth and Planetary Science Letters* **53**, 189–202.

Deplus, C., Bonavalot, S., Dahrain, D., Diament, M., Harjono, H. & Dubois, J. (1995). Inner structure of the Krakatau volcanic complex (Indonesia) from gravity and bathymetry data. *Journal of Volcanology and Geothermal Research* **64**, 23–52.

Diament, M., Deplus, C., Harjono, H., Larue, M., Lassal, O., Dubois, J. & Renard, V. (1990). Extension in the Sunda Strait (Indonesia): a review of the Krakatau programme. *Oceanologia Acta* **10**, 31–41.

Diament, M., Harjono, H., Karta, K., Deplus, C., Dahrin, D., Zen, M. T., Jr, Gérard, M., Lassal, O., Martin, A. & Malod, J. (1992). Mentawai fault zone off Sumatra: a new key to the geodynamics of western Indonesia. *Geology* **20**, 259–262.

Donoghue, E., Troll, V. R., Harris, C., O'Halloran, A., Walter, T. R. & Pérez Tòrrado, F. J. (2008). Low-temperature hydrothermal alteration of intra-caldera tuffs, Miocene Tejeda caldera, Gran Canaria, Canary Islands. *Journal of Volcanology and Geothermal Research* **176**, 551–564.

Dufek, J. & Bergantz, G. W. (2005). Lower crustal magma genesis and preservation: a stochastic framework for the evaluation of basalt–crust interaction. *Journal of Petrology* **46**, 2167–2195.

Dungan, M. (2005). Partial melting at the Earth's surface: implications for assimilation rates and mechanisms in subvolcanic intrusions. *Journal of Volcanology and Geothermal Research* **140**, 193–203.

Eiler, J. M. (2001). Oxygen isotope variations of basaltic lavas and upper mantle rocks. In: Valley, J. W. & Cole, D. R. (eds) *Stable Isotope Geochemistry. Mineralogical Society of America and Geochemical Society. Reviews in Mineralogy and Geochemistry* **43**, 319–364.

Eiler, J. M., Crawford, A., Elliott, T., Farley, K. A., Valley, J. W. & Stolper, E. M. (2000). Oxygen isotope geochemistry of oceanic-arc lavas. *Journal of Petrology* **41**, 229–256.

Elsworth, D., Mattioli, G., Taron, J., Voight, B. & Herd, R. (2008). Implications of magma transfer between multiple reservoirs on eruption cycling. *Science* **322**, 246–248.

Escher, B. G. (1919). *Excursie-gids voor Krakatau, Samengesteld voor de Excursie. Samengesteld voorde Excursie, te houden door het Eerste Nederlandsch-Indisch Natuurwetenschappelijk Congres*. Weltevreden: Albrecht **7** p.

Escher, B. G. (1928). Krakatau in 1883 and in 1928. *Tijdschrift van het Koninklijk Nederlandsch Aardriikskundig Genootschap* **45**, 715–743.

Feeley, T. C. & Sharp, Z. D. (1995). $^{18}O/^{16}O$ isotope geochemistry of silicic lava flows erupted from Volcán Ollagüe, Andean Central Volcanic Zone. *Earth and Planetary Science Letters* **133**, 239–254.

Fitton, J. G. & Godard, M. (2004). Origin and evolution of magmas on the Ontong Java Plateau. In: Fitton, J. G., Mahoney, J. J., Wallace, P. J. & Saunders, A. D. (eds) *Origin and Evolution of the Ontong Java Plateau. Geological Society, London, Special Publications* **229**, 151–178.

Fitton, J. G., Saunders, A. D., Larsen, L. M., Hardarson, B. S. & Norry, M. J. (1998). Volcanic rocks from the East Greenland margin at 63°N: composition, petrogenesis and mantle sources. In: Saunders, A. D., Larsen, H. C. & Wise, S. H. (eds) *Proceedings of the Ocean Drilling Program, Scientific Results, 152*. College Station, TX: Ocean Drilling Program, pp. 331–350.

Francalanci, L., Davies, G. R., Lustenhouwer, W., Tommasini, S., Mason, P. R. D. & Conticelli, S. (2005). Intra-grain Sr isotope evidence for crystal recycling and multiple magma reservoirs in the recent activity of Stromboli Volcano, Southern Italy. *Journal of Petrology* **46**, 1997–2021.

Francis, P. W. & Self, S. (1983). The eruption of Krakatau. *Scientific American* **249**, 172–187.

Gamble, J. A., Wood, C. P., Price, R. C., Smith, I. E. M., Stewart, R. B. & Waight, T. (1999). A fifty-year perspective of magmatic evolution on Ruapehu volcano, New Zealand: Verification of open system behaviour in an arc volcano. *Earth and Planetary Science Letters* **170**, 301–314.

Gasparon, M., Hilton, D. R. & Varne, R. (1994). Crustal contamination processes traced by helium isotopes: examples from the Sunda arc, Indonesia. *Earth and Planetary Science Letters* **126**, 15–22.

Ginibre, C. & Wörner, G. (2007). Variable parent magmas and recharge regimes of the Parinacota magma system (N. Chile) revealed by Fe, Mg and Sr zoning in plagioclase. *Lithos* **98**, 118–140.

Ginibre, C., Wörner, G. & Kronz, A. (2002). Minor- and trace-element zoning in plagioclase: implications for magma chamber processes at Parinacota Volcano, northern Chile. *Contributions to Mineralogy and Petrology* **143**, 300–315.

Grapes, R. (2006). *Pyrometamorphism*. Berlin: Springer.

Grove, T. L., Baker, M. B. & Kinzler, R. J. (1984). Coupled CaAl–NaSi diffusion in plagioclase feldspar: experiments and applications to cooling rate speedometry. *Geochimica et Cosmochimica Acta* **48**, 2113–2121.

Hamilton, W. B. (1979). *Tectonics of the Indonesian Region*, US Geological Survey Professional Papers 1078.

Hansteen, T. H. & Troll, V. R. (2003). Oxygen isotope composition of xenoliths from the oceanic crust and volcanic edifice beneath Gran Canaria (Canary Islands): consequences for crustal contamination of ascending magmas. *Chemical Geology* **193**, 181–193.

Hanuš, V., Špičák, A. & Vaněk, J. (1996). Sumatran segment of the Indonesian subduction zone: morphology of the Wadati–Benioff zone and seismotectonic pattern of the continental wedge. *Journal of Southeast Asian Sciences* **13**, 39–60.

Harjono, H., Diament, M., Nouali, L. & Dubois, J. (1989). Detection of magma bodies beneath Krakatau volcano (Indonesia) from anomalous shear waves. *Journal of Volcanology and Geothermal Research* **39**, 335–348.

Harjono, H., Diament, M., Dubois, J., Larue, M. & Zen, M. T. (1991). Seismicity of the Sunda Strait: evidence for crustal extension and volcanological implications. *Tectonics* **10**, 17–30.

Harris, C., Smith, H. S. & le Roex, A. P. (2000). Oxygen isotope composition of phenocrysts from Tristan da Cunha and Gough Island

lavas: variation with fractional crystallisation and evidence for assimilation. *Contributions to Mineralogy and Petrology* **138**, 164–175.

Hildreth, H. H. & Moorbath, S. (1988). Crustal contributions to arc magmatism in the Andes of central Chile. *Contributions to Mineralogy and Petrology* **98**, 455–489.

Hoffman-Rothe, A., Ibs-von Seht, M., Knieß, R., Faber, E., Klinge, K., Reichert, C., Purbawinata, M. A. & Patria, C. (2006). Monitoring Anak Krakatau volcano in Indonesia. *EOS Transactions American Geophysical Union* **87**, 581–586.

Huchon, P. & Le Pichon, X. (1984). Sunda Strait and Central Sumatra Fault. *Geology* **12**, 668–672.

Humphreys, M. C. S., Blundy, J. D. & Sparks, R. S. J. (2006). Magma evolution and open-system processes at Shiveluch Volcano: insights from phenocryst zoning. *Journal of Petrology* **47**, 2303–2334.

Ibs-von Seht, M. (2008). Detection and identification of seismic signals recorded at Krakatau volcano (Indonesia) using artificial neural networks. *Journal of Volcanology and Geothermal Research* **176**, 448–456.

Jarrard, R. D. (1986). Relation among subduction parameters. *Reviews of Geophysics* **24**, 217–284.

Jaxybulatov, K., Koulakov, I., Ibs-von Seht, M., Klinge, K., Reichart, C., Dahren, B. & Troll, V. R. (2011). Evidence for high fluid/melt content beneath Krakatau volcano (Indonesia) from local earthquake tomography. *Journal of Volcanology and Geothermal Research* **206**, 96–105.

Jicha, B. R., Singer, B. S., Beard, B. L. & Johnson, C. M. (2005). Contrasting timescales of crystallisation and magma storage beneath the Aleutian Island arc. *Earth and Planetary Science Letters* **236**, 195–210.

Judd, J. W. (1889). The earlier eruptions of Krakatau. *Nature* **40**, 365–366.

Knesel, K. M., Davidson, J. P. & Duffield, W. A. (1999). Open-system evolution of silicic magma by assimilation followed by recharge: evidence from Sr isotopes in sanidine phenocrysts, Taylor Creek rhyolite, New Mexico. *Journal of Petrology* **40**, 773–786.

Kopp, H., Flueh, E. R., Klaeschen, D., Bialas, J. & Reichert, C. (2001). Crustal structure of the central Sunda margin at the onset of oblique subduction. *Geophysical Journal International* **147**, 449–474.

Lassal, O., Huchon, P. & Harjono, H. (1989). Extension crustale dans le détroit de la Sonde (Indonésie): Données de la sismique réflexion (Campagne Krakatau). *Comptes Rendus de l'Académie des Sciences* **309**, 205–212.

Lelgemann, H., Gutscher, M., Bialas, J., Flueh, E., Weinrebe, W. & Reichert, C. (2000). Transtensional basins in the western Sunda Strait. *Geophysical Research Letters* **27**, 3545–3548.

Lunt, P., Burgon, G. & Baky, A. (2009). The Pemali Formation of Central Java and equivalents: Indicators of sedimentation on an active plate margin. *Journal of Asian Earth Sciences* **34**, 100–113.

Malod, J. A. & Kemal, B. M. (1996). The Sumatra margin: oblique subduction and lateral displacement of the accretionary prism. In: Hall, R. & Blundell, D. J. (eds) *Tectonic Evolution of South East Asia. Geological Society, London, Special Publications* **106**, 19–28.

Malod, J. A., Karta, K., Beslier, M. O. & Zen, M. T., Jr (1995). From normal to oblique subduction: tectonic relationships between Java and Sumatra. *Journal of Southeast Asian Earth Sciences* **12**, 85–93.

Mandeville, C. W., Carey, S. & Sigurdsson, H. (1996). Magma mixing, fractional crystallization and volatile degassing during the 1883 eruption of Krakatau volcano, Indonesia. *Journal of Volcanology and Geothermal Research* **74**, 243–274.

Metcalfe, I. (1990). Allochthonous terrane processes in Southeast Asia. *Philosophical Transactions of the Royal Society of London* **331**, 625–640.

Metcalfe, I. (2011). Tectonic framework and Phanerozoic evolution of Sundaland. *Gondwana Research* **19**, 3–21.

Meyer, R., Nicoll, G. R., Hertogen, J., Troll, V. R., Ellam, R. M. & Emeleus, C. H. (2009). Trace element and isotope constraints on crustal anatexis by upwelling mantle melts in the North Atlantic Igneous Province: an example from the Isle of Rum, NW Scotland. *Geological Magazine* **146**, 382–399.

Morgan, D. J., Jerram, D. A., Chertkoff, D. G., Davidson, J. P., Pearson, D. G., Kronz, A. & Nowell, G. M. (2007). Combining CSD and isotopic microanalysis: Magma supply and mixing processes at Stromboli Volcano, Aeolian Islands, Italy. *Earth and Planetary Science Letters* **260**, 419–431.

Nakagawa, M., Wada, K., Thordarson, T., Wood, C. P. & Gamble, J. A. (1999). Petrologic investigations of the 1995 and 1996 eruptions of Ruapehu volcano, New Zealand: formation of discrete and small magma pockets and their intermittent discharge. *Bulletin of Volcanology* **61**, 15–31.

Newcomb, K. R. & McCann, W. R. (1987). Seismic history and seismotectonics of the Sunda Arc. *Journal of Geophysical Research* **92**, 421–439.

Nishimura, S., Ikeda, T. & Ishizaka, K. (1980). Geochemistry in volcanic rocks of Krakatau, Indonesia. In: Nishimura, S. (ed.) *Physical Geology of Indonesian Island Arcs*. Kyoto University, pp. 109–113.

Nishimura, S., Nishida, J., Yokoyama, T. & Hebuwat, F. (1986). Neo-tectonics of the Strait of Sunda, Indonesia. *Journal of Southeast Asian Earth Sciences* **1**, 81–91.

Noujaim, A. (1976). Drilling in a high temperature and overpressured area Sunda Straits, Indonesia. *Proceedings of the Fifth Annual Convention of Indonesian Petrological Association, Jakarta*, pp. 211–214.

Oba, N., Tomita, K., Yamamoto, M., Istidjab, M., Badruddin, M., Parlin, M., Sadjiman, , Djuwandi, A., Sudradjat, A. & Suhanda, T. (1982). Geochemical study of lava flows, ejecta and pyroclastic flow from the Krakatau Group, Indonesia. *Reports of the Faculty of Science, Kagoshima University (Earth Science and Biology)* **15**, 41–76.

Oba, N., Tomita, K. & Yamamoto, M. (1992). An interpretation of the 1883 cataclysmic eruption of Krakatau from geochemical studies on the partial melting of granite. *GeoJournal* **28**, 99–108.

Olive, V., Ellam, R. M. & Wilson, L. (2001). A protocol for the determination of the rare earth elements at picomole level in rocks by ICP-MS: results on geological reference materials USGS PCC-1 and DTS-1 2001. *Geostandards Newsletter* **25**, 219–228.

Pearce, T. H. & Kolisnik, A. M. (1990). Observations of plagioclase zoning using interference imaging. *Earth-Science Reviews* **29**, 275–289.

Pichavant, M., Costa, F., Burgisser, A., Scaillet, B., Martel, C. & Poussineau, S. (2007). Equilibration scales in silicic to intermediate magmas—implications for experimental studies. *Journal of Petrology* **48**, 1955–1972.

Pouchou, J.-L. & Pichoir, F. (1991). Quantitative analysis of homogeneous or stratified microvolumes applying the model of 'PAP'. In: Heinrich, K. F. J. & Newbury, D. E. (eds) *Electron Probe Quantitation*. New York: Plenum, pp. 31–76.

Price, R. C., Gamble, J. A., Smith, I. E. M., Stewart, R. B., Eggins, S. & Wright, I. C. (2005). An integrated model for the temporal evolution of andesites and rhyolites and crustal development in New Zealand's North Island. *Journal of Volcanology and Geothermal Research* **140**, 1–24.

Ramos, F. C., Wolff, J. A. & Tollstrup, D. L. (2004). Measuring $^{87}Sr/^{86}Sr$ variations in minerals and groundmass from basalts using LA-MC-ICPMS. *Chemical Geology* **211**, 135–158.

Ramos, F. C., Wolff, J. A. & Tollstrup, D. L. (2005). Sr isotope disequilibrium in Columbia River flood basalts: Evidence for rapid shallow-level open-system processes. *Geology* **33**, 457–460.

Renzulli, A., Tribaudino, M., Salvioli-Mariani, E., Serri, G. & Holm, P. M. (2003). Cordierite–anorthoclase hornfels xenoliths in Stromboli lavas (Aeolian Islands, Sicily): an example of a fast cooled contact aureole. *European Journal of Mineralogy* **15**, 665–679.

Reubi, O. & Blundy, J. (2009). A dearth of intermediate melts at subduction zone volcanoes and the petrogenesis of arc andesites. *Nature* **461**, 1269–1274.

Ruprecht, P. & Wörner, G. (2007). Variable regimes in magma systems documented in plagioclase zoning patterns: El Misti stratovolcano and Andahua monogenetic cones. *Journal of Volcanology and Geothermal Research* **165**, 142–162.

Ruprecht, P., Bergantz, G. W. & Dufek, J. (2008). Modeling of gas-driven magmatic overturn: Tracking of phenocryst dispersal and gathering during magma mixing. *Geochemistry, Geophysics, Geosystems* **9(7)**, Q07017, doi:10.1029/2008GC002022.

Schlüter, H. U., Gaedicke, C., Roeser, H. A., Schreckenberger, B., Meyer, H., Reichert, C., Djajadihardja, Y. & Prexl, A. (2002). Tectonic features of the southern Sumatra–western Java forearc of Indonesia. *Tectonics* **21(5)**, 1047, doi:10.1029/2001TC901048.

Self, S. & Rampino, M. R. (1981). The 1883 eruption of Krakatau. *Nature* **294**, 699–704.

Sigurdsson, H., Carey, S., Mandeville, C. & Bronto, S. (1991). Pyroclastic flows of the 1883 Krakatau eruption. *EOS Transactions American Geophysical Union* **72**, 380–381.

Simkin, T & Fiske, R. S. (eds) (1983). *Krakatau, 1883—the Volcanic Eruption and its Effects*. Washington, DC: Smithsonian Institution Press.

Singer, B. S., Dungan, M. A. & Layne, G. D. (1995). Textures and Sr, Ba, Fe, K and Ti compositional profiles in volcanic plagioclase: clues to the dynamics of calc-alkaline magma chambers. *American Mineralogist* **80**, 776–798.

Spera, F. J. & Bohrson, W. A. (2001). Energy-constrained open-system magmatic processes I: general model and energy-constrained assimilation–fractional crystallization (EC-AFC) formulation. *Journal of Petrology* **42**, 999–1018.

Špičák, A., Hanuš, V. & Vaněk, J. (2002). Seismic activity around and under Krakatau volcano, Sunda Arc: Constraints to the source region of island arc volcanics. *Studia Geophysica et Geodaetica* **40**, 545–565.

Stamatelopoulou-Seymour, K., Vlassapoulos, D., Pearce, T. H. & Rice, C. (1990). The record of magma chamber processes in plagioclase at Thera volcano, Aegean volcanic arc, Greece. *Contributions to Mineralogy and Petrology* **104**, 73–84.

Stehn, C. E. (1929). The geology and volcanism of the Krakatau Group. *Proceedings of the 4th Pacific Science Congress*, Batavia, 1–55.

Sudradjat (Samartadipura), A. (1982). The morphological development of Anak Krakatau volcano, Sunda Strait. *Geologi Indonesia* **9**, 1–11.

Sun, S.-S. & McDonough, W. F. (1989). Chemical and isotopic systematics of oceanic basalts: implications for mantle composition and processes. *Geological Society, London, Special Publications* **42**, 313–345.

Susilohadi, S., Gaedicke, C. & Djajadihardja, Y. (2009). Structures and sedimentary deposition in the Sunda Strait, Indonesia. *Tectonophysics* **467**, 55–71.

Taylor, H. P., Jr. & Sheppard, S. M. F. (1986). Igneous rocks: I. Processes of isotopic fractionation and isotopic systematics, in Valley, J. W., Taylor, H. P., O'Neil, J. R. (eds) Stable isotopes in high temperature geological processes. *Mineralogical Society of America, Reviews in Mineralogy* **16**, Washington, D.C., pp. 227–271.

Tepley, F. J., III, Davidson, J. P. & Clynne, M. A. (1999). Magmatic interactions as recorded in plagioclase phenocrysts of Chaos Crags, Lassen Volcanic Center, California. *Journal of Petrology* **40**, 787–806.

Tepley, F. J., III, Davidson, J. P., Tilling, R. I. & Arth, J. G. (2000). Magma mixing, recharge, and eruption histories recorded in plagioclase phenocrysts from El Chichón Volcano, Mexico. *Journal of Petrology* **41**, 1397–1411.

Thirlwall, M. F. (1991). Long-term reproducibility of multicollector Sr and Nd isotope ratio analysis. *Chemical Geology* **94**, 85–104.

Troll, V. R., Donaldson, C. H. & Emeleus, C. H. (2004). Pre-eruptive magma mixing mixing in intra-caldera ash-flow deposits of the Rum Igneous Centre, Scotland. *Contributions to Mineralogy and Petrology* **147**, 722–739.

Troll, V. R., Chawick, J. P., Ellam, R. M., McDonnell, S., Emeleus, C. H. & Meighan, I. G. (2005). Sr and Nd isotope evidence for successive crustal contamination of Slieve Gullion ring-dyke magmas, Co. Armagh, Ireland. *Geological Magazine* **142**, 659–668.

Troll, V. R., Klügel, A., Longpré, M.-A., Burchardt, S., Deegan, F. M., Carracedo, J. C., Wiesmaier, S., Kueppers, U., Dahren, B., Blythe, L. S., Hansteen, T., Freda, C., Budd, D. A., Jolis, E. M., Jonsson, E., Meade, F., Harris, C., Berg, S., Mancini, L., Polacci, M. & Pedroza, K. (2012). Floating stones off El Hierro, Canary Islands: xenoliths of pre-island sedimentary origin in the early products of the October 2011 eruption. *Solid Earth* **3**, 97–110.

Turner, S. & Foden, J. (2001). U, Th, and Ra disequilibria, Sr, Nd and Pb isotope and trace element variations in Sunda arc lavas: predominance of a subdusted sediment component. *Contributions to Mineralogy and Petrology* **142**, 43–57.

Van Bemmelen, R. W. (1949). *The Geology of Indonesia. 1A, General Geology*. The Hague: Government Printing Office.

Verbeek, R. D. M. (1884). The Krakatoa eruption. *Nature* **30**, 10–15.

Verbeek, R. D. M. (1885). *Krakatau*. Batavia: Landsdrukkerij, 495 p.

Wakita, K. (2000). Cretaceous accretionary–collision complexes in central Indonesia. *Journal of Asian Earth Sciences* **18**, 739–749.

Wallace, G. S. & Bergantz, G. W. (2005). Reconciling heterogeneity in crystal zoning data: An application of shared characteristic diagrams at Chaos Crags, Lassen Volcanic Center. *Contributions to Mineralogy and Petrology* **149**, 98–112.

Weiss, S. & Troll, G. (1989). The Ballachulish Igneous Complex, Scotland: Petrography, mineral chemistry, and order of crystallisation in the monzonite–quartz diorite suite and in the granite. *Journal of Petrology* **30**, 1069–1115.

Whitford, D. J. (1975). Strontium isotopic studies of the volcanic rocks of the Sunda arc, Indonesia, and their petrogenetic implications. *Geochimica et Cosmochimica Acta* **39**, 1287–1302.

Williams, I. S., Cho, D. L. & Kim, S. W. (2009). Geochronology, and geochemical and Nd–Sr isotopic characteristics, of Triassic plutonic rocks in the Gyeonggi Massif, South Korea: constraints on Triassic post-collision magmatism. *Lithos* **107**, 239–256.

Woodhead, J. D., Hergt, J. M., Davidson, J. P. & Eggins, S. M. (2001). Hafnium isotope evidence for 'conservative' element mobility during subduction zone processes. *Earth and Planetary Science Letters* **192**, 331–346.

Zellmer, G. F., Blake, S., Vance, D., Hawkesworth, C. & Turner, S. (1999). Plagioclase residence times at two island arc volcanoes (Kameni islands, Santorini, and Soufrière, St. Vincent) determined by Sr diffusion systematics. *Contributions to Mineralogy and Petrology* **136**, 345–357.

Zellmer, G. F., Sparks, R. S. J., Hawkesworth, C. J. & Wiedenbeck, M. (2003). Magma emplacement and remobilization timescales beneath Montserrat: insights from Sr and Ba zonation in plagioclase phenocrysts. *Journal of Petrology* **44**, 1413–1431.